HAL
open science

Geometric chaos indicators, computations, and guided visualizations of the spherical hypertube manifolds of the spatial circular restricted three-body problem

Massimiliano Guzzo, Elena Lega

To cite this version:

Massimiliano Guzzo, Elena Lega. Geometric chaos indicators, computations, and guided visualizations of the spherical hypertube manifolds of the spatial circular restricted three-body problem. 2016. hal-01343970v1

HAL Id: hal-01343970

https://hal.science/hal-01343970v1

Preprint submitted on 11 Jul 2016 (v1), last revised 6 Apr 2017 (v2)

HAL is a multi-disciplinary open access archive for the deposit and dissemination of scientific research documents, whether they are published or not. The documents may come from teaching and research institutions in France or abroad, or from public or private research centers.

L'archive ouverte pluridisciplinaire **HAL**, est destinée au dépôt et à la diffusion de documents scientifiques de niveau recherche, publiés ou non, émanant des établissements d'enseignement et de recherche français ou étrangers, des laboratoires publics ou privés.

Geometric chaos indicators, computations, and guided visualizations of the spherical hypertube manifolds of the spatial circular restricted three-body problem

Massimiliano Guzzo
Università degli Studi di Padova
Dipartimento di Matematica
Via Trieste, 63 - 35121 Padova, Italy

Elena Lega
Laboratoire Lagrange, Université Côte d'Azur
Observatoire de la Côte d'Azur, CNRS
Blvd de l'Observatoire, CS 34229,
06304 Nice cedex 4, France

July 6, 2016

Abstract

The circular restricted three-body problem has five relative equilibria L_1, L_2, ..., L_5. The invariant stable-unstable manifolds of the center manifolds originating at the partially hyperbolic equilibria L_1,L_2 have been identified as the separatrices for the motions which transit between the regions of the phase–space which are internal or external with respect to the two massive bodies. This paper is devoted to the global computation of these manifolds in the spatial case with a suitable finite time chaos indicator. The definition of the chaos indicator is not trivial, since the mandatory use of the regularizing Kustaanheimo-Stiefel variables introduces branch discontinuities in the individual Lyapunov indicators. From the study of such discontinuities, we define geometric chaos indicators which are smooth, globally defined, and whose ridges sharply approximate the stable and unstable manifolds of the center manifolds of L_1, L_2. We illustrate the method for the Sun-Jupiter mass ratio, and represent the topology of the asymptotic manifolds using sections and three-dimensional representations.

1 Introduction

The circular restricted three-body problem describes the motion of a massless body P in the gravitation field of two massive bodies P_1 and P_2, called primary and secondary body respectively, which rotate uniformly around their common center of mass. In a rotating frame the problem has five equilibria, the so called Lagrangian points $L_1, \ldots, L_5$, which are the only known simple solutions of the

equations of motion of P:

$$\begin{cases} \ddot{x} &= 2\dot{y} + x - (1-\mu)\frac{x+\mu}{r_1^3} - \mu\frac{x-1+\mu}{r_2^3} \\ \ddot{y} &= -2\dot{x} + y - (1-\mu)\frac{y}{r_1^3} - \mu\frac{y}{r_2^3} \\ \ddot{z} &= -(1-\mu)\frac{z}{r_1^3} - \mu\frac{z}{r_2^3} \quad , \end{cases} \tag{1}$$

where the units of masses, lengths and time have been chosen so that the masses of P_1 and P_2 are $1-\mu$ and μ ($\mu \leq 1/2$) respectively, their coordinates are $(-\mu, 0, 0)$ and $(1-\mu, 0, 0)$ and their revolution period is 2π; we denoted by $r_1 = \sqrt{(x+\mu)^2 + y^2 + z^2}$ and by $r_2 = \sqrt{(x-1+\mu)^2 + y^2 + z^2}$ the distances of P from P_1, P_2. As it is well known, equations (1) have an integral of motion, the so–called Jacobi constant, defined by:

$$\mathcal{C}(x, y, z, \dot{x}, \dot{y}, \dot{z}) = x^2 + y^2 + 2\frac{1-\mu}{r_1} + 2\frac{\mu}{r_2} - \dot{x}^2 - \dot{y}^2 - \dot{z}^2. \tag{2}$$

Fixed values C of the Jacobi constant define level sets $\mathcal{M}_C$ in the phase-space, which project on the set:

$$\Pi\mathcal{M}_C = \{(x, y, z) \in \mathbb{R}_0^3 : x^2 + y^2 + 2\frac{1-\mu}{r_1} + 2\frac{\mu}{r_2} \geq C\}$$

of the physical space:

$$\mathbb{R}_0^3 = \{(x, y, z) \in \mathbb{R}^3 : (x, y, z) \neq (-\mu, 0, 0), (1-\mu, 0, 0)\}.$$

The boundary $\mathcal{B}_C$ of $\Pi\mathcal{M}_C$ separates the so called realm of possible motions $\Pi\mathcal{M}_C$ from the realm of forbidden motions $\mathbb{R}_0^3 \backslash \Pi\mathcal{M}_C$.

The Lagrangian equilibria $L_1, \ldots, L_5$ are critical points for the Jacobi constant; the values $C_1, C_2, ..., C_5$ of $\mathcal{C}$ at the Lagrangian equilibria $L_1, \ldots, L_5$ correspond to topological changes of the set $\mathcal{B}_C$. In particular, for $C > C_2$ the space $\mathbb{R}_0^3$ is disconnected by $\mathcal{B}_C$ into a region of motions which contains the massive bodied P_1, P_2 and an external region; for $C < C_2$ the realm of possible motions is connected; in particular, for values of C slightly smaller than C_2, the connection between the internal and external regions is realized through a bottleneck of $\mathcal{B}_C$, at whose extremities we find the Lagrangian points L_1 and L_2. The transit of motions through this bottleneck is guided by the stable-unstable manifolds of the center manifolds W_1^c, W_2^c originating at the equilibria L_1,L_2, which are partially hyperbolic, specifically they are saddle$\times$center$\times$center. The center manifold theorem (see, for example, [32]) grants the existence of two four-dimensional center manifolds W_i^c, $i = 1, 2$. Since the restriction of the Jacobi constant to each W_i^C has a strict extremum at the equilibrium point L_i, from the general results of [32] we obtain that the center manifolds of L_1 and L_2 are unique, and for suitably small values of $C - C_2$ the sets $W_{C,i}^c = W_i^c \cap \mathcal{M}_C$, which are diffeomorphic to a three-sphere, are invariant with respect to the flow of the three-body problem for any time $t \in \mathbb{R}$. Also, both manifolds $W_{C,i}^c$ are normally hyperbolic and have stable and unstable manifolds holding the topology of hypertubes obtained from the

product of a three-sphere with an half line; we will call them spherical hypertube manifolds. The spherical hypertube manifolds act as separatrices for the transit of motions through the bottleneck of $\mathcal{B}_C$ connecting the region of internal and the region of external motions, see [4, 33, 16] (for the planar three-body problem) and [9] (for the spatial three-body problem). This fact is a consequence of the structure of the local stable-unstable manifolds of $W^c_{C,i}$ in a small neighbourhood $\mathcal{U}_i$: motions with initial conditions in $\mathcal{U}_i$ approaching the center manifold from the right-hand side (left-hand side respectively) 'bounce back' if they are on one side of the separatrix, while they transit to the left-hand side (right-hand side respectively) if they are on the other side of the separatrix.

The structure of the global stable and unstable manifolds of $W^c_{C,i}$ is much more complicate than the structure of the local manifolds: the exponential compressions, expansions and rotations occurring near the center manifolds are alternated to circulations around both primaries. Global representations of these surfaces have been obtained for several sample values of μ and C in the planar circular restricted three-body problem, see for example [16, 13, 24]. The computation of the stable-unstable manifolds in the planar case has several advantages with respect to the spatial case. First, in the planar case, the level set of the center manifolds obtained by fixing the value of the Jacobi constant in a suitable small left neighbourhood of C_i is made of a periodic orbit, the horizontal Lyapunov orbit of L_1 or L_2. To compute their asymptotic manifolds one can use one of the several methods of computation of the stable and unstable manifolds of periodic orbits, for example the flow continuation of the local manifolds, the parametrization method, or the recent method based on chaos indicators (see [13] and the references therein). Moreover, the phase-space of the planar three-body problem is four dimensional, and by fixing the value of the Jacobi constant we obtain a three dimensional space. The stable and unstable manifolds of the horizontal Lyapunov orbits are therefore two-dimensional surfaces in a three-dimensional space; their global phase-space development has been graphically visualized in [24].

In this paper we provide a method, based on the computation of chaos indicators, to compute and represent the global structure of the stable-unstable manifolds of $W^c_{C,i}$ in the spatial circular restricted three-body problem. While the computation of the stable and unstable manifolds of equilibria and of periodic orbits has been considered in many papers, much less attention has been devoted to the computation of the stable and unstable manifolds of center manifolds of higher dimension. Our method applies independently on the dimension of the center manifold, provided that it is globally invariant with respect to the flow: first, we construct a neighbourhood $\mathcal{U}_i$ of the center manifold $W^c_{C,i}$ where the local stable and unstable manifolds are represented as Cartesian graphs and an hyperbolic Birkhoff normal form of some convenient order is defined; then, we localize the global stable manifold $W^s_{C,i}$ by exploiting at the same time the peculiar growth of the tangent vectors close to $W^c_{C,i}$, and the scattering from $\mathcal{U}_i$ of the motions with initial conditions outside the local stable manifold. Both

properties are coded by a finite time chaos indicator, fast Lyapunov indicator or finite time Lyapunov indicator, whose ridges provide the stable manifold[1] $W^s_{C,i}$.

The definition of smooth chaos indicators for the spatial three-body problem is non trivial since equations (1) are singular for $(x, y, z) = (-\mu, 0, 0)$ or $(1-\mu, 0, 0)$. Smooth equations of motions are defined by using the Kustaanheimo-Stiefel regularization (KS hereafter, [17, 18]). The KS transformation had been originally introduced to regularize the spatial Kepler problem; afterwards, it was used to regularize also the equations of motions of N-body problems (see [29, 1, 3] and also [2] and the references therein); in particular the equations of motions of the spatial circular restricted three-body problem have been regularized at the secondary, or alternatively at the primary, body (for details, see [6]). The use of regularizing transformations, with their analytic and computational advantages (see, for example, [2, 28, 36]) appear to us mandatory to compute long pieces of the spherical hypertube manifolds of L_1, L_2, especially close to the secondary body. In this spirit, the Levi-Civita transformation (LC hereafter), which regularizes the equations of motion of the planar three-body problem [26], has been used in [13, 24] to define chaos indicators whose ridges approximate the stable and unstable manifolds of the horizontal Lyapunov orbits of L_1, L_2. Even if the KS transformation is the natural extension of the LC transformation, the spatial problem is intrinsically more complicate than the planar one. On the one hand, we show that as a consequence of Sundman's proper time transformation [35] used in KS and LC transformation, for both regularizations the solutions of the variational equations written in the Cartesian phase-space are not conjugate to the solutions of the variational equations written in the KS or LC variables, so that the Lyapunov exponents (as well as other chaos indicators) defined with the regularized variational equations are different functions from the chaos indicators defined with the non-regularized variational equations. On the other hand, the redundancy of the Kustaanheimo-Stiefel variables introduces a symmetry, degenerate at the singularity, whose consequence is twofold: two additional Lyapunov exponents are introduced; the chaos indicators defined by the KS-regularized variational equations for orbits corresponding the the same initial conditions of the physical phase-space and the same initial tangent vector have branch discontinuities. A careful analysis of these branch discontinuities allows us to define 'geometric' chaos indicators, which are globally defined and smooth on the Cartesian phase-space, and to suitably select a family of branched indicators whose ridges approximate the stable and unstable manifolds of $W^c_{C,i}$, to conveniently use for the numerical applications.

Once the suitable chaos indicators are defined, we set up a method to represent the global development in the phase-space of the hypertube manifolds. The most important problem is related to the dimension of the hypertubes and of the invariant set $\mathcal{M}_C$ they belong to. Our first choice is to compute and represent

[1] As usual, the unstable manifold $W^u_{C,i}$ is obtained by computing the stable manifold of the inverse flow.

sections of the hypertubes, which provide us the knowledge of how these manifolds intersect well chosen two-dimensional surfaces transverse to it. Because of the symmetry of the three-body problem, the first condition to define a good section is to set: $y = 0$. In the planar problem the condition $y = 0$ defines the two-dimensional surface in $\mathcal{M}_C$:

$$\Sigma_P = \{(x, y, z, \dot{x}, \dot{y}, \dot{z}) : y = z = 0, \dot{z} = 0, \mathcal{C}(x, 0, \dot{x}, \dot{y}, 0) = C\}. \tag{3}$$

which we call the planar section. In the planar section there are peculiar initial conditions, characterized by $\dot{x} = 0$, whose orbits satisfy a well known time reversal symmetry. In particular, if they belong to the stable manifold of L_1 or L_2, they are homoclinic. The vertical section:

$$\Sigma_V = \{(x, y, z, \dot{x}, \dot{y}, \dot{z}) : y = 0, \dot{x} = \dot{z} = 0, \mathcal{C}(x, 0, \dot{x}, \dot{y}, 0) = C\} \tag{4}$$

intersects the planar section Σ_P exactly on its line $\dot{x} = 0$. The homoclinic planar orbits of L_i on this axes are continued in Σ_V to curves of initial conditions on homoclinic orbits of the center manifold $W^c_{C,i}$. In fact, we remark that all motions $(x(t), y(t), z(t))$ with $(x(0), y(0), z(0), \dot{x}(0), \dot{y}(0), \dot{z}(0)) \in \Sigma_V$ satisfy the time–reversal symmetry (also $(x(-t), -y(-t), z(-t))$ is a solution of equations (1)). Moreover, from the mirror theorem [30], if an orbit hits the section in at least two points, then it is a periodic orbit and therefore cannot belong to a stable or unstable manifold. As a consequence, the vertical section is not redundant: all the points of $W^s \cap \Sigma$ are not connected by orbits.

We will compute several connected components of $W^s_{C,i} \cap \Sigma_V$ of both Lagrangian points L_1, L_2, in the realms of motions around the primary and secondary body respectively. To define precisely the realms of motions for $C < C_2$ we find useful to consider isolating blocks at L_1, L_2 [5, 27] of equations:

$$R_1 = \{(x, y, z, \dot{x}, \dot{y}, \dot{z}) \in \mathcal{M}_C : x \in [x_1, x_2]\}$$

$$R_2 = \{(x, y, z, \dot{x}, \dot{y}, \dot{z}) \in \mathcal{M}_C : x \in [x_3, x_4]\}$$

where $x_1 < x_{L_1} < x_2$, $x_3 < x_{L_2} < x_4$, while we have:

$$x - (1-\mu)\frac{x+\mu}{r_1^3} - \mu\frac{x-1+\mu}{r_2^3} < -2\sqrt{x^2 + y^2 + 2\frac{(1-\mu)}{r_1} + 2\frac{\mu}{r_2} - C}$$

for all $(x_1, y, z) \in \Pi\mathcal{M}_C$ and $(x_3, y, z) \in \Pi\mathcal{M}_C$, and:

$$x - (1-\mu)\frac{x+\mu}{r_1^3} - \mu\frac{x-1+\mu}{r_2^3} > 2\sqrt{x^2 + y^2 + 2\frac{(1-\mu)}{r_1} + 2\frac{\mu}{r_2} - C}$$

for all $(x_2, y, z) \in \Pi\mathcal{M}_C$ and $(x_4, y, z) \in \Pi\mathcal{M}_C$. The two conditions are found so that any orbit hitting the border of R_1 or R_2 from the left (resp. from the right) tangentially, i.e. with $\dot{x} = 0$, bounces back because $\ddot{x} < 0$ (resp. because

$\ddot{x} > 0$). The center manifolds $W^c_{C,i}$ are contained in the isolating blocks R_i and, by taking x_1, x_3 as large as possible and x_2, x_4 as small as possible (within their numerical error determination), we define the realms S, J, E of motions around the primary, around the secondary mass[2] and external to the binary system P_1P_2 by (see figure 1)

$$\begin{array}{rcl} S & = & \Pi\{(x,y,z,\dot{x},\dot{y},\dot{z}) \in \mathcal{M}_C : x < x_1\} \\ J & = & \Pi\{(x,y,z,\dot{x},\dot{y},\dot{z}) \in \mathcal{M}_C : x \in (x_2, x_3)\} \\ E & = & \Pi\{(x,y,z,\dot{x},\dot{y},\dot{z}) \in \mathcal{M}_C : x > x_4\} \end{array} \tag{5}$$

respectively.

The connected components of $W^s_{C,i} \cap \Sigma_V$ of both Lagrangian points L_1, L_2, will be denoted by Λ^i_j if they are in the realm J of motions around the secondary mass; $i = 1$ or $i = 2$ depending on the Lagrangian point L_1, L_2; $j = 1, 2 \ldots$ is a label for the connected component; the components will be denoted by M^1_j if they are in the realm S of motions around the primary mass defined by $x \leq x_1$.

Since we find that the Λ^i_j are closed, and since the spherical hypertube manifolds are separatrices for the transit from/to the realm of motions S, J and E, all the initial conditions of Σ_V which are in the interior of Λ^1_j transit from J to S in the same number of revolutions $(j-1)/2$ around the secondary mass P_2; similarly we find that the initial conditions of Σ_V which are in the interior of Λ^2_j transit from J to E in the same number of revolutions $(j-1)/2$ around the secondary mass P_2. The transits of the orbits with initial conditions in Σ_V which are external to a given Λ^i_j is not determined, since we find that a curve Λ^i_j can be connected by the stable manifold $W^s_{C,i}$ to other curves $\tilde{\Lambda}^i_j$ through the five-dimensional space $\mathcal{M}_C$ which $W^s_{C,i}$ belongs to, and all the initial conditions in the interiors of both $\Lambda^i_j, \tilde{\Lambda}^i_j$ transit from J to S in the same number of revolutions around P_2. Similarly, we compute closed curves M^1_j, whose interior points transits from S to J after the same number of revolutions around P_1. The transits from J to S (or from S to J) and from J to E need a passage through the isolating blocks R_1, R_2 respectively.

The article is structured as follows. In Section 2 we discuss the properties of the variational equations of the restricted three-body problem defined from the KS variables; in Section 3 we discuss the branch discontinuities of chaos indicators and we define geometric chaos indicators which are globally defined and smooth on the Cartesian phase-space as well as a family of branched indicators to conveniently use for numerical computations; in Section 4 we show that the ridges of the previously defined chaos indicators approximate the stable and unstable manifolds of $W^c_{C,i}$; in Section 5 we provide the explicit definition of the smooth weight functions entering the definitions of the chaos indicators; in Sections 6 we provide example of computations of the manifolds for the Sun-Jupiter

[2]The realm of motions around P_1 and P_2 are denoted by S, J respectively, since we conventionally identify P_1 with the Sun and P_2 with Jupiter.

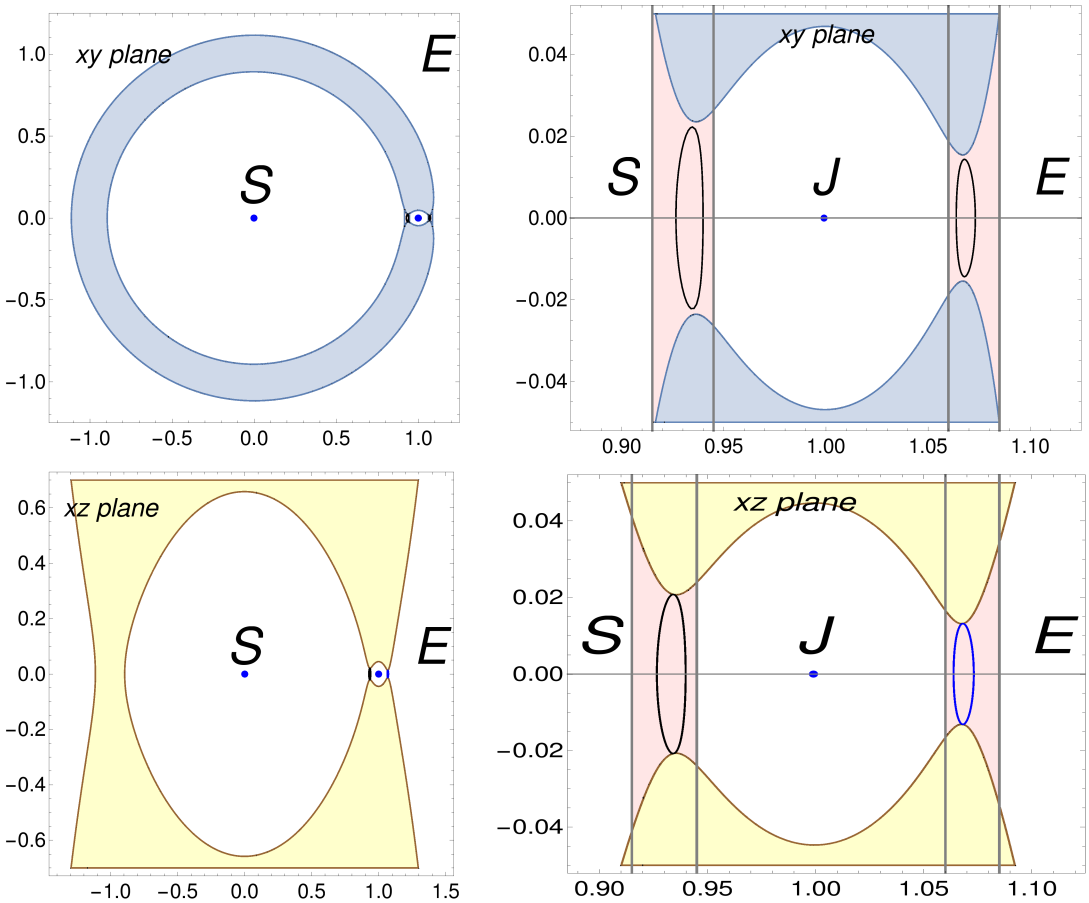

Figure 1: **Representation of the realms of motion S, J, E and of the isolating blocks** R_1, R_2 in the x, y plane ($z = 0$), top panels, and in the x, z plane ($y = 0$), bottom panels, for a value of the Jacobi constant, slightly smaller than C_2. The right panels are obtained as a zoom at P_2 of the left panels. The vertical gray lines, located at $x = x_1, x_2, x_3, x_4$, represent the boundaries of two isolating blocks R_1, R_2 containing the center manifolds of L_1 and L_2 for the same value C of the Jacobi constant. The black curves in the x, y plane represent the horizontal Lyapunov orbits of L_1, L_2, while the blue curves in the x, z plane represent the intersections of center manifolds of L_1, L_2 with the vertical section Σ_V (computed as explained in Section 6).

mass ratio and we discuss the dynamics of orbits with initial conditions in the vertical section Σ_V; in Section 7 we provide some Conclusions.

2 The Kustaanheimo-Stiefel regularization at the secondary body: variational equations and linearizations

In this Section we discuss the properties of the variational equations of the restricted three-body problem defined from the KS variables. First, we review the KS transformation regularizing the equations of motions of the three–body problem; then we discuss the invariance properties of the solutions of the variational equations of the regularized equations of motion, and compare them with the solutions of the variational equations of the non-regularized equations of motion.

2.1 The KS transformation

The Kustaanheimo-Stiefel regularization at the secondary body P_2 is defined by the introduction of redundant spatial variables $u = (u_1, u_2, u_3, u_4)$ related to the Cartesian variables (x, y, z) by:

$$\left\{ \begin{array}{rcl} x & = & 1 - \mu + u_1^2 - u_2^2 - u_3^2 + u_4^2 \\ y & = & 2(u_1 u_2 - u_3 u_4) \\ z & = & 2(u_1 u_3 + u_2 u_4) \end{array} \right. \tag{6}$$

and by the time transformation [35]:

$$dt = r_2 ds \tag{7}$$

where t denotes the physical time, and s is called the proper time. The map defined by equations (6), a particular case of Hopf transformation [21], will be denoted by:

$$\begin{array}{rcl} \pi : \mathbb{U} & \longrightarrow & \mathbb{R}^3 \\ (u_1, u_2, u_3, u_4) & \longmapsto & \pi(u_1, u_2, u_3, u_4) = (x, y, z), \end{array} \tag{8}$$

where $\mathbb{U}$ denotes the space of the $u = (u_1, u_2, u_3, u_4)$ variables. As usual, we also find convenient to consider the four dimensional extension of (8):

$$\begin{array}{c} \tilde{\pi} : \ \mathbb{U} \longrightarrow \mathbb{R}^4 \\ u \longmapsto (x, y, z, q) = A(u)u \end{array} \tag{9}$$

with:

$$A(u) = \begin{pmatrix} u_1 & -u_2 & -u_3 & u_4 \\ u_2 & u_1 & -u_4 & -u_3 \\ u_3 & u_4 & u_1 & u_2 \\ u_4 & -u_3 & u_2 & -u_1 \end{pmatrix}. \tag{10}$$

With evidence, any $u \in \mathbb{U}$ is mapped to some $\tilde{\pi}(u) = (x, y, z, q)$ with $q = 0$.

For a fixed value C of the Jacobi constant, the equations of motion of the spatial restricted three-body problem in the variables u and proper time s are[3] (see, for example, [6]):

$$\left\{\begin{array}{rcl} u_1'' & = & (K_1+K_2)u_1+K_3u_2-K_4u_3 \\ u_2'' & = & (K_1-K_2)u_2+K_3u_1-K_4u_4 \\ u_3'' & = & (K_1-K_2)u_3-K_3u_4-K_4u_1 \\ u_4'' & = & (K_1+K_2)u_4-K_3u_3-K_4u_2 \end{array}\right. \tag{11}$$

with:

$$\begin{array}{rcl} K_1 & = & \frac{1}{4}\left(\frac{2(1-\mu)}{r_1}-C+x^2+y^2\right) \\ K_2 & = & \frac{1}{4}\left(4y'+2r_2x-\frac{2(1-\mu)r_2(x+\mu)}{r_1^3}\right) \\ K_3 & = & \frac{1}{4}\left(2r_2y-4x'-\frac{2mr_2y}{r_1^3}\right) \\ K_4 & = & \frac{1}{4}\left(\frac{2(1-\mu)r_2z}{r_1^3}\right) \end{array}$$

regular functions at $u=0$ (x,y,z,x',y',r_1,r_2 are expressed using $u_1,\ldots,u_4$, $u_1',\ldots,u_4'$), complemented with the non holonomic constraint:

$$u\cdot\Omega u'=0 \quad , \quad \Omega=\left(\begin{array}{cccc} 0 & 0 & 0 & 1 \\ 0 & 0 & -1 & 0 \\ 0 & 1 & 0 & 0 \\ -1 & 0 & 0 & 0 \end{array}\right). \tag{12}$$

In the following, we denote by $\xi=(x,y,z,v_x,v_y,v_z)\in T\mathbb{R}^3$ the Cartesian phase-space variables, by $\zeta=(u,\nu)\in T\mathbb{U}=\mathbb{R}^8$ the Kustaanheimo Stiefel phase-space variables and by:

$$\begin{array}{c} \mathcal{X}:\ T\mathbb{U}_0\longrightarrow T\mathbb{R}^3 \\ \zeta\longmapsto\xi=\mathcal{X}(\zeta) \end{array} \tag{13}$$

the transformation between them defined by:

$$\begin{array}{rcl} x & = & 1-\mu+u_1^2-u_2^2-u_3^2+u_4^2 \\ y & = & 2(u_1u_2-u_3u_4) \\ z & = & 2(u_1u_3+u_2u_4) \\ v_x & = & \frac{2}{\|u\|^2}\left(u_1\nu_1-u_2\nu_2-u_3\nu_3+u_4\nu_4\right) \\ v_y & = & \frac{2}{\|u\|^2}\left(u_1\nu_2+\nu_1u_2-u_3\nu_4-\nu_3u_4\right) \\ v_z & = & \frac{2}{\|u\|^2}\left(u_1\nu_3+\nu_1u_3+u_2\nu_4+\nu_2u_4\right). \end{array} \tag{14}$$

[3]The primes denote derivatives with respect to the proper time s.

where[4] $\mathbb{U}_0 = \mathbb{U}\backslash 0$. Transformation (14) is immediately extended to:

$$\begin{array}{rcl} \tilde{\chi}: \ T\mathbb{U}_0 & \longrightarrow & \mathbb{R}^8 \\ (u_1, u_2, u_3, u_4, \nu_1, \nu_2, \nu_3, \nu_4) & \longmapsto & (x, y, z, q, v_x, v_y, v_z, v_q) \end{array} \tag{15}$$

with:

$$\begin{array}{c} (x, y, z, q) = A(u)u \\ (v_x, v_y, v_z, v_q) = \frac{1}{\|u\|^2}\left(A(u)\nu + A(\nu)u\right) = \frac{2}{\|u\|^2}A(u)\nu \quad , \end{array} \tag{16}$$

where the last equality in the second line of (16) has been obtained for $u \cdot \Omega\nu = 0$; notice that the (u, ν) satisfying the non-holonomic relation $u \cdot \Omega\nu = 0$ project to some $(x, y, z, q, v_x, v_y, v_z, v_q)$ with $v_q = 0$.

The solutions of equations (11) and the solutions of equations (1) are conjugate, in the following sense (again, for the details, see [6]):

Proposition 0. *Let us consider a solution $u(s)$ of equations (11), with initial conditions $(u(0), u'(0))$ satisfying equations (12), defined in some neighbourhood $\mathcal{S}$ of $s = 0$ with $\pi(u(s)) \neq (-\mu, 0, 0), (1-\mu, 0, 0)$ for all $s \in \mathcal{S}$; denote by:*

$$t(s) = \int_0^s \|u(\sigma)\|^2 \, d\sigma, \tag{17}$$

and consider the solutions $(x(t), y(t), z(t))$ of (1) with initial conditions:

$$(x(0), y(0), z(0), \dot{x}(0), \dot{y}(0), \dot{z}(0)) = \chi(u(0), u'(0)).$$

We have:

$$(x(t(s)), y(t(s)), z(t(s))) = \pi(u(s)) \qquad \forall \ \ s \in \mathcal{S}.$$

The inverse of the KS transformation (6), and of its phase-space extension (14), are undetermined: in fact the projection $\chi(u, \nu)$ of any $(u, \nu) \in T\mathbb{U}_0$ on the Cartesian variables $(x, y, z, \dot{x}, \dot{y}, \dot{z})$ is invariant under the transformation:

$$u \mapsto \mathcal{R}_\alpha u \quad , \quad \nu \mapsto \mathcal{R}_\alpha \nu \tag{18}$$

where:

$$\mathcal{R}_\alpha = \begin{pmatrix} \cos\alpha & 0 & 0 & -\sin\alpha \\ 0 & \cos\alpha & \sin\alpha & 0 \\ 0 & -\sin\alpha & \cos\alpha & 0 \\ \sin\alpha & 0 & 0 & \cos\alpha \end{pmatrix}, \tag{19}$$

for all $\alpha \in [0, 2\pi]$. In particular, the pre-image of the Lagrangian points L_1, L_2 defined by the map χ is the set of the $(u, \nu) := (u^*(\alpha), 0)$ with:

$$\begin{array}{l} u_1^*(\alpha) = u_4^*(\alpha) = 0 \ , \ u_2^*(\alpha) = \sqrt{\gamma_1}\cos\alpha \ , \ u_3^*(\alpha) = \sqrt{\gamma_1}\sin\alpha \ (\text{for } L_1) \\ u_2^*(\alpha) = u_3^*(\alpha) = 0 \ , \ u_1^*(\alpha) = \sqrt{\gamma_2}\cos\alpha \ , \ u_4^*(\alpha) = \sqrt{\gamma_2}\sin\alpha \ (\text{for } L_2) \end{array} \tag{20}$$

where $\alpha \in [0, 2\pi]$, and γ_1, γ_2 denote the Cartesian distances of the equilibria configurations L_1, L_2 from P_2.

[4]Since we are interested only in the solutions $u(s)$ of (11) which project to solutions of (1), the restriction to $\mathbb{U}_0$ is allowed.

2.2 Tangent map of the KS phase-space transformation

The tangent map of (15) defines a projection from the space of vectors tangent to $T\mathbb{U}_0$ to the space of vectors tangent to $T\mathbb{R}^8$. Precisely, for any $(u,\nu) \in T\mathbb{U}_0$ with $u \cdot \Omega\nu = 0$, consider the map:

$$\begin{array}{rcl} D\tilde{\chi}_{(u,\nu)} : \ T_{(u,\nu)}T\mathbb{U}_0 & \longrightarrow & T_{\tilde{\chi}(u,\nu)}\mathbb{R}^8 \\ w := (w_u, w_\nu) & \longmapsto & V = (V_r, V_v) \end{array} \tag{21}$$

defined by:

$$\begin{pmatrix} V_r \\ V_v \end{pmatrix} = \begin{pmatrix} A(u)w_u + A(w_u)u \\ \frac{2}{\|u\|^2}\left(A(w_u)\nu + A(u)w_\nu - \frac{2}{\|u\|^2}u \cdot w_u A(u)\nu\right) \end{pmatrix}. \tag{22}$$

Because of the non-holonomic constraint $u \cdot \Omega\nu = 0$, we restrict the tangent map (22) to the set:

$$\hat{T}_{(u,\nu)}T\mathbb{U}_0 = \{(w_u, w_\nu) \in T_{(u,\nu)}T\mathbb{U}_0 \ : \ u \cdot \Omega w_\nu + w_u \cdot \Omega\nu = 0\}. \tag{23}$$

The inverse of $D\tilde{\chi}_{(u,\nu)}$ is undetermined; the indetermination is fixed by choosing a smooth local inversion of π. Let us in fact consider a smooth local inversion of the map (8):

$$\begin{array}{c} \pi^{-1} : \mathcal{W} \longrightarrow \mathbb{U}_0 \\ (x,y,z) \longmapsto u = \pi^{-1}(x,y,z), \end{array} \tag{24}$$

with $\mathcal{W}$ open set. The choice of π^{-1} uniquely fixes the inversion of equations (9), by providing:

$$\begin{array}{rcl} u & = & \pi^{-1}(x,y,z) \\ \nu & = & \dfrac{1}{2}A^T(u)(v_x, v_y, v_z, 0), \end{array} \tag{25}$$

and, for tangent vectors $(V_r, V_v) \in \mathbb{R}^8$ with $V_q, V_{v_q} = 0$, also the inversion of equations (22):

$$\begin{array}{rcl} w_u & = & JV_r \\ w_v & = & \dfrac{1}{2}A^T(u)V_v - \dfrac{1}{\|u\|^2}A^T(u)A(w_u)\nu + \dfrac{2}{\|u\|^2}u \cdot w_u\nu \end{array} \tag{26}$$

where J is the Jacobian matrix of the map $(x,y,z,q) \mapsto u = \pi^{-1}(x,y,z)$, computed at $(x,y,z,0)$ (u,ν in the right hand side of (26) are obtained from (25)).

2.3 Variational equations of the restricted three-body problem

The conjugation (Proposition 0) between the solutions of equations (1) and the solutions of equations (11) does not extend to their variational equations. In

fact, let us first consider the variational equations of the regularized equations of motion (11), which are obtained from the first order differential equations:

$$\begin{cases} u_i' &= \nu_i,\ i=1,\dots,4 \\ \nu_1' &= (K_1+K_2)u_1 + K_3u_2 - K_4u_3 \\ \nu_2' &= (K_1-K_2)u_2 + K_3u_1 - K_4u_4 \\ \nu_3' &= (K_1-K_2)u_3 - K_3u_4 - K_4u_1 \\ \nu_4' &= (K_1+K_2)u_4 - K_3u_3 - K_4u_2 \end{cases}$$

denoted in compact form by:

$$\zeta' = F_C(\zeta) \tag{27}$$

with $\zeta = (u_1,\dots,u_4,\nu_1,\dots,\nu_4)$. We notice that the vector field $F_C(\zeta)$ is invariant with respect to the transformation $R_\alpha\zeta = (\mathcal{R}_\alpha u, \mathcal{R}_\alpha v)$, i.e. we have:

$$F_C(\zeta) = R_\alpha^T F_C(R_\alpha\zeta). \tag{28}$$

For any solution $\zeta(s)$ of (27) we define the variational equations:

$$w' = \frac{\partial F_C}{\partial \zeta}(\zeta(s))w, \tag{29}$$

where $w = (w_u, w_\nu) \in TT\mathbb{U}$ is a vector tangent to the domain of the Kustaanheimo Stiefel phase-space variables ζ. Then, we consider the variational equations of the non-regularized equations of motion (1), obtained from the first order differential equations in the extended Cartesian space $\mathbb{R}^8$:

$$\begin{cases} \dot{x} &= v_x \\ \dot{y} &= v_y \\ \dot{z} &= v_z \\ \dot{q} &= v_q \\ \dot{v_x} &= 2v_y + x - (1-\mu)\frac{x+\mu}{r_1^3} - \mu\frac{x-1+\mu}{r_2^3} \\ \dot{v_y} &= -2v_x + y - (1-\mu)\frac{y}{r_1^3} - \mu\frac{y}{r_2^3} \\ \dot{v_z} &= -(1-\mu)\frac{z}{r_1^3} - \mu\frac{z}{r_2^3} \quad , \\ \dot{v_q} &= 0 \end{cases}$$

denoted in a compact form by:

$$\dot{\xi} = \Xi(\xi) \tag{30}$$

where, with a little abuse of notation, we denote $\xi = (r, v) = (x, y, z, q, \dot{x}, \dot{y}, \dot{z}, \dot{q})$; the extension to the (q, v_q) variables is conveniently introduced to simplify the reference to the projection (22), of course we will only consider solutions with $q(t) = 0, v_q(t) = 0$. For any solution $\xi(t)$ of (30) we obtain the variational equations:

$$\dot{V} = \frac{\partial \Xi}{\partial \xi}(\xi(t))V, \tag{31}$$

where $V = (V_r, V_v)$. We prove the following:

Proposition 1. *Let us consider a non constant solution $u(s)$ of equations (11) with initial conditions $(u(0), u'(0))$ satisfying condition (12), defined in some neighbourhood $\mathcal{S}$ of $s = 0$ with $\pi(u(s)) \neq (-\mu, 0, 0), (1-\mu, 0, 0)$ for all $s \in \mathcal{S}$; denote by:*

$$t(s) = \int_0^s \|u(\sigma)\|^2 \, d\sigma, \tag{32}$$

and by $(x(t), y(t), z(t))$ the solution of (1) such that $(x(t(s)), y(t(s)), z(t(s))) = \pi(u(s))$ for all $s \in \mathcal{S}$. Then:

(i) there exist solutions $w(s) = (w_u(s), w_\nu(s))$ of (29) defined by $\zeta(s) = (u(s), u'(s))$, with some $w(0) \in \hat{T}T\mathbb{U}$, such that by denoting with $V(t) = (V_r(t), V_v(t))$ the functions of time defined by $V(t(s)) = D\tilde{\chi}_{(u(s),\nu(s))}(w_u(s), w_\nu(s))$ for all $s \in \mathcal{S}$, $V(t)$ is not a solution of (31).
(ii) let us consider a matrix $B(\zeta)$ such that, for any solution $\zeta(s)$ of (27) and for all the solutions $w(s)$ of the differential equation:

$$w' = B(\zeta(s))w,$$

the functions of time defined by $V(t(s)) = D\tilde{\chi}_{(u(s),\nu(s))}(w_u(s), w_\nu(s))$ are solutions of (31) with $\xi(t(s)) = \tilde{\chi}(\zeta(s))$. Then, the matrix $B(\zeta)$ is singular at $u = 0$.

From (i), we have that the variational equations of (1) are not conjugate by the KS transformation to the variational equations of the regularized equations of motion (11). This apparent contradiction is due to the fact that the Kustaanheimo Stiefel transformation, including the proper time transformation, is not simply a transformations of variables and therefore the usual conjugation of variational equations under smooth changes of variables does not apply. In particular, the chaos indicators constructed from the solutions of the variational equations, such as the Lyapunov exponents, the fast Lyapunov indicators, the finite time Lyapunov exponents, are different if they are defined from the solutions of (29) or from the solutions of (31). From (ii), we have that the equation conjugate to (31) is singular; i.e. the KS transformation regularizes the equations of motions, not the variational equations.

We are therefore faced with a choice: is it more convenient to define chaos indicators from the smooth variational equations (29) or from the singular equations (31)? The choice of using the chaos indicators defined by the smooth variational equations (29) appears as mandatory. In fact, the numerical integration of the singular variational equations introduces very strong numerical instabilities[5] already in the planar case (see [23]), which instead are completely under control using equations (29). On the other hand, the definition of chaos indicators using the evolution of the tangent vectors in the KS variables introduces a subtle geometric problem, which is analyzed in Section 3.

[5]The variational equations (31) have singularities of higher order with respect to the singularities of the equations of motion, since they are obtained by further differentiating the singular terms $1/r_1^3$, $1/r_2^3$.

Proof of Proposition 1. For any solution $w(s) = (w_u(s), w_\nu(s))$ of (29) with $w(0) \in \hat{T}T\mathbb{U}$, since $u \cdot \Omega\nu$ is a first integral of equations (27), we have $w(s) \in \hat{T}T\mathbb{U}$ for all $s \in \mathcal{S}$. Let us consider the functions of time $V(t) = (V_r(t), V_v(t))$ such that $V(t(s)) = D\tilde{\chi}_{(u(s),\nu(s))}(w_u(s), w_\nu(s))$ for all s. By computing the time derivative of $V_r(t)$, and using $w_u' = w_\nu$, we obtain:

$$\dot{V}_r = \frac{1}{\|u\|^2}\left(A(u)w_\nu + A(\nu)w_u + A(w_\nu)u + A(w_u)\nu\right),$$

or equivalently:

$$\dot{V}_r = V_v + \frac{4}{\|u\|^4} u \cdot w_u A(u)\nu.$$

Instead, the solutions $\tilde{V}(t)$ of (31) satisfy $\dot{\tilde{V}}_r = \tilde{V}_v$. Therefore, if we have:

$$u(s) \cdot w_u(s) A(u(s))\nu(s) \neq 0$$

for some s, $V(t)$ does not solve (31). We remark that since the solution $u(s)$ is not constant, and $u(s) \neq 0$, we have $A(u(s))\nu(s) \neq 0$ in an open subset $\tilde{\mathcal{S}}$ of $\mathcal{S}$. Therefore, if there exists $s \in \tilde{S}$ such that $u(s) \cdot w_u(s) \neq 0$, $V(t)$ does not solve (31). We now consider $w(0)$ such that $u(0) \cdot w_u(0) \neq 0$. Then, in a neighbourhood of $s = 0$, we find $s \in \mathcal{S}$ where both $u(s) \cdot w_u(s) \neq 0$ and $A(u(s))\nu(s) \neq 0$. This proves that solutions $w(s)$ of the variational equations (29) do not project on the solutions of the variational equations (31).

Then, let us suppose that the solutions of the differential equation:

$$(w_u', w_\nu') = B(u(s), \nu(s))(w_u, w_\nu) \tag{33}$$

project on the solution of the variational equations (31). Precisely, by defining $V(t) = (V_r(t), V_v(t))$ such that $V(t(s)) = D\tilde{\chi}_{(u(s),\nu(s))}(w_u(s), w_\nu(s))$, then $V(t)$ satisfies (31). First, we notice that by computing the time derivative of $V_r(t)$ we obtain:

$$\dot{V}_r = \frac{1}{\|u\|^2}\left(A(u)w_u' + A(\nu)w_u + A(w_u')u + A(w_u)\nu\right).$$

From:

$$\dot{V}_r = V_v = \frac{1}{\|u\|^2}\left(A(u)w_\nu + A(w_u)\nu + A(w_\nu)u + A(\nu)w_u - \frac{4u \cdot w_u}{\|u\|^2}A(u)\nu\right)$$

we obtain that, along all the solutions $w(s)$ of (33) we have

$$A(u)w_u' + A(w_u')u = A(u)w_\nu + A(w_\nu)u - \frac{4u \cdot w_u}{\|u\|^2}A(u)\nu,$$

and therefore the matrix $B(\zeta)$ satisfies:

$$A(u)[B(\zeta)w]_u + A([B(\zeta)w]_u)u = A(u)w_\nu + A(w_\nu)u - \frac{4u \cdot w_u}{\|u\|^2}A(u)\nu.$$

If the matrix $B(\zeta)$ is regular at $u = 0$, by taking the limit of u tending to zero for constant ν, w of the previous equation we obtain:

$$\lim_{u \to 0} \frac{4u \cdot w_u}{\|u\|^2} A(u)\nu = 0$$

which is not satisfied for certain choices of ν, w_u. $\square$

2.4 Linearizations in the space of KS variables

We need to establish some invariance properties of the Jacobian matrix $\frac{\partial F_C}{\partial \zeta}$ and of the solutions of the variational equations (29) with respect to the symmetry transformation (18). First, from the invariance relations (28), we obtain:

$$\frac{\partial F_C}{\partial \zeta}(\zeta) = R_\alpha^T \frac{\partial F_C}{\partial \zeta}(R_\alpha \zeta) R_\alpha \tag{34}$$

for any α and ζ. As a consequence, by denoting with $\zeta(s), w(s)$ the solutions of the equations (27) and (29) with initial conditions ζ_0, w_0, then $R_\alpha \zeta(s), R_\alpha w(s)$ are the solutions of (29) with initial conditions $R_\alpha \zeta_0, R_\alpha w_0$. This invariance will be used to define a chaos indicator invariant by the transformation $\zeta \mapsto R_\alpha \zeta$.

As a consequence of (34), the eigenvalues of the Jacobian matrices $\frac{\partial F_C}{\partial \zeta}(\zeta)$ are invariant by the transformation $\zeta \mapsto R_\alpha \zeta$; i.e. they depend only on the projection $\mathcal{X}(\zeta)$. In particular, at all $\zeta = (u^*(\alpha), 0)$, corresponding to the representatives (20) of the Lagrangian points L_1, L_2, the matrix:

$$F_{C,\alpha} = \frac{\partial F_C}{\partial \zeta}(u^*(\alpha), 0), \tag{35}$$

has eigenvalues which are independent of α for all the values of C: for $C = C_i$ ($i = 1, 2$ for L_1 or L_2) the matrices $F_{C_i,\alpha}$ have a pair of real eigenvalues $\pm\lambda^0 \neq 0$, two pairs of purely complex eigenvalues $\pm i\sigma_j^0$, $j = 1, 2$, and an additional eigenvalue $\lambda = 0$ of multiplicity 2; we also prove that[6] for any fixed value of μ and $C = C_i - \varepsilon$, with suitably small $\varepsilon > 0$, the matrix $F_{C,\alpha}$ has a pair of real eigenvalues $\pm\lambda^\varepsilon$, two pairs of purely complex eigenvalues $\pm i\sigma_j^\varepsilon$, $j = 1, 2$, and the real pair $\pm\sqrt{\varepsilon}/2$.

In fact, by considering the linearization at L_1 (the case of L_2 is similar) for $C = C_1 - \varepsilon$ with $\varepsilon > 0$, since the eigenvalues are invariant with respect to the parameter α, we only compute the eigenvalues of the matrix:

$$F_{C,0} = \begin{pmatrix} O & \mathcal{I}_4 \\ \mathcal{A} & \mathcal{B} \end{pmatrix} \tag{36}$$

[6]Since we will consider the dynamics in small neighbourhoods of L_1 (or L_2) for values of the Jacobi constant smaller than C_1 (or C_2), we will consider expansions of $\frac{\partial F_C}{\partial \zeta}(\zeta)$ at $\zeta = (u^*(\alpha), 0)$ also for $C < C_i$.

where O is a 4×4 square matrix with entries $O_{ij} = 0$, for $i, j = 1, \ldots, 4$; $\mathcal{I}_4$ is the 4×4 identity matrix, the matrices $\mathcal{A}$, $\mathcal{B}$ are defined by:

$$\mathcal{A} = \begin{pmatrix} a & 0 & 0 & 0 \\ 0 & b & 0 & 0 \\ 0 & 0 & c & 0 \\ 0 & 0 & 0 & d \end{pmatrix} \quad , \quad \mathcal{B} = \begin{pmatrix} 0 & 2\gamma_1 & 0 & 0 \\ -2\gamma_1 & 0 & 0 & 0 \\ 0 & 0 & 0 & 0 \\ 0 & 0 & 0 & 0 \end{pmatrix} \tag{37}$$

where:

$$\begin{aligned} a &= \frac{\varepsilon}{4} - \gamma_1^2 \frac{3 + \gamma_1^2 - 2\gamma_1^3 + \gamma_1^4}{\gamma} \\ b &= \frac{\varepsilon}{4} - \gamma_1^2 \frac{-9 + 6\gamma_1 - 5\gamma_1^2 - 2\gamma_1^3 + \gamma_1^4}{\gamma} \\ c &= \frac{\varepsilon}{4} \\ d &= \frac{\varepsilon}{4} - 2\gamma_1^2 \frac{2 - \gamma_1 + \gamma_1^2}{\gamma} \\ \gamma &= 1 - 2\gamma_1 + \gamma_1^2 + 2\gamma_1^3 - \gamma_1^4. \end{aligned} \tag{38}$$

The characteristic equation determining the eigenvalues λ of (36):

$$\det(\mathcal{A} + \lambda\mathcal{B} - \lambda^2 \mathcal{I}_4) = 0 \tag{39}$$

can be represented in the form:

$$\frac{1}{\gamma^2}\left(\frac{\varepsilon}{4} - \lambda^2\right)\left(-\frac{2\gamma_1^2(2 - \gamma_1 + \gamma_1^2)}{\gamma} + \frac{\varepsilon}{4} - \lambda^2\right)(R_1 + R_2\lambda^2 + R_3\lambda^4) = 0.$$

where R_1, R_2 are coefficients depending only on γ_1, ε and R_3 dependent only of γ_1. Therefore, four eigenvalues are:

$$\begin{aligned} \lambda_{1,2} &= \pm\sqrt{\varepsilon} \\ \lambda_{3,4} &= \pm i\sqrt{\frac{2\gamma_1^2(2 - \gamma_1 + \gamma_1^2)}{\gamma} - \frac{\varepsilon}{4}} \end{aligned} \tag{40}$$

while the other four eigenvalues are:

$$\lambda_{5,6,7,8} = \pm\sqrt{\frac{-R_2 \pm \sqrt{R_2^2 - 4R_1R_3}}{2R_3}}. \tag{41}$$

Since for small ε we have $R_2 < 0$, $R_3 > 0$, and $R_1R_3 < 0$, two of the eigenvalues (41) are opposite real numbers, the other two are opposite purely imaginary numbers.

Remark 1. The explicit computations of Section 6 will be done for values of μ corresponding the the Sun-Jupiter system and a value of the Jacobi constant $C = 3.03685...$; correspondingly we have:

$$\frac{2\gamma_1^2(2 - \gamma_1 + \gamma_1^2)}{\gamma} - \frac{\varepsilon}{4} > 0$$

as well as $R_2 < 0$, $R_3 > 0$, and $R_1R_3 < 0$, so that the above analysis is applicable.

3 Geometric chaos indicators for the spatial restricted three-body problem

The solutions $w(s)$ of the variational equations (29) enter the definition of the chaos indicators which we use to compute the hypertube manifolds of the spatial restricted three-body problem. Through all this section, by ϕ we denote any fixed non negative smooth function:

$$\phi : \mathcal{M}_C \longrightarrow [0, +\infty).$$

Definition 1. *For any $\xi_0 = (x_0, y_0, z_0, \dot{x}_0, \dot{y}_0, \dot{z}_0) \in \mathcal{M}_C$ we consider a smooth pre-image of χ:*

$$\zeta = \chi^{-1}(\xi) = (\pi^{-1}(x, y, z), \tilde{\pi}^{-1}(\xi))$$

defined in a neighbourhood $\mathcal{W}$ of ξ_0. Then, for any positive time $T > 0$, we define the modified finite time Lyapunov exponent (mFTLE hereafter):

$$\mathcal{F}_\phi^T : \mathcal{W} \longrightarrow \mathbb{R} \tag{42}$$

by:

$$\mathcal{F}_\phi^T(\xi) = \max_{t\in[0,T]} \max_{w_0\in\mathbb{R}^8, \|w_0\|=1} \int_0^{\sigma(\xi,t)} \phi(\mathcal{X}(\zeta(s)) \frac{w(s) \cdot w'(s)}{\|w(s)\|^2} ds. \tag{43}$$

where $\zeta(s)$ is the solution of equations (27) with initial condition $\zeta(0) = \chi^{-1}(\xi)$; $w(s)$ is the solution of the variational equations (29) defined by $\zeta(s)$ with initial conditions $w(0) = w_0$; $\sigma(\xi, t)$ denotes the transformation $s := \sigma(\xi, t)$ between any physical time t and the proper time s for the orbit with initial conditions ξ.

Equation (43) provides a local definition for the mFTLE, since it depends on the specific choice of the local inversion function χ^{-1}. Since we have to compute the chaos indicators in extended domains of the phase-space, we need to consider global extensions. A non trivial property of the function defined in (43) is that its values are independent on the specific choices of χ^{-1}, In fact, we have the following

Theorem 1. *For any value C of the Jacobi constant and for any $T > 0$, consider any open set $\mathcal{M}_{C,T} \subseteq \mathcal{M}_C$ such that the solution $(x(t), y(t), z(t))$ of (1) with initial conditions $(x(0), y(0), z(0), \dot{x}(0), \dot{y}(0), \dot{z}(0)) \in \mathcal{M}_{C,T}$ exist with $(x(t), y(t), z(t)) \in \mathbb{R}^3_0$ for all $t \in [0, T]$. Then, any local definition of the modified finite fime Lyapunov exponent obtained from (43) has a unique smooth global extension to $\mathcal{M}_{C,T}$.*

Proof of Theorem 1. The proof is obtained from two lemmas: in Lemma 1 we establish the uniqueness of the mFTLE in the intersection of the domains of any two smooth local inversions; in Lemma 2, we define a covering of $\mathcal{M}_{C,T}$ with two smooth local inversions.

Lemma 1. *Let us consider two smooth local inversions:*

$$\chi_1{}^{-1} : \mathcal{W}_1 \to T\mathbb{U} \quad , \quad \chi_2{}^{-1} : \mathcal{W}_2 \to T\mathbb{U}$$

of the map $\xi = \chi(\zeta)$, with $\mathcal{W}_1, \mathcal{W}_2$ open sets with non empty intersection $\mathcal{W} = \mathcal{W}_1 \cap \mathcal{W}_2$ satisfying[7] *$\Pi\mathcal{W}_1, \Pi\mathcal{W}_2 \subseteq \mathbb{R}^3_0$. For any $T > 0$ consider the modified finite time Lyapunov exponents $\mathcal{F}^T_{1,\phi}$, $\mathcal{F}^T_{2,\phi}$ defined by (43), using the local inversion χ_1^{-1}, χ_2^{-1} respectively. For any $\xi \in \mathcal{W} \cap \mathcal{M}_C$ we have:*

$$\mathcal{F}^T_{1,\phi}(\xi) = \mathcal{F}^T_{2,\phi}(\xi).$$

Because of Lemma 1, equation (43) defines a global phase-space function, which is smooth on any domain $\mathcal{W}$ where motions with initial conditions in $\mathcal{W}$ do not collide with the primary of the secondary body for $t \in [0, T]$.

Proof of Lemma 1. The proof of the Lemma is obtained from the invariance properties (28) and (34). In fact, let us consider the transition map:

$$\begin{array}{rcl} \mathcal{X}_{1,2} : \chi_1^{-1}(\mathcal{W}) & \longrightarrow & \chi_2^{-1}(\mathcal{W}) \\ \zeta = (u, v) & \longmapsto & \tilde{\zeta} = (\tilde{u}, \tilde{v}) = \mathcal{X}_{1,2}(\zeta). \end{array} \tag{44}$$

There exists $\alpha \in [0, 2\pi)$, depending only on $(x, y, z) = \chi_1(u, v) = \chi_2(\tilde{u}, \tilde{v})$, such that: $(\tilde{u}, \tilde{v}) = (\mathcal{R}_\alpha u, \mathcal{R}_\alpha v)$. In fact, let us split $u \in \mathbb{U}$ on the following two-dimensional projections:

$$U = (u_1, u_4), \quad V = (u_2, u_3),$$

so that we have:

$$\begin{array}{rcl} \|U\|^2 - \|V\|^2 & = & X \\ \|U\|^2 + \|V\|^2 & = & \sqrt{X^2 + y^2 + z^2}, \end{array} \tag{45}$$

where $X = x - (1 - \mu)$, as well as:

$$\begin{array}{rcl} \|U\| & = & \dfrac{1}{\sqrt{2}} \sqrt{\sqrt{X^2 + y^2 + z^2} + X} \\ \|V\| & = & \dfrac{1}{\sqrt{2}} \sqrt{\sqrt{X^2 + y^2 + z^2} - X}. \end{array} \tag{46}$$

The preimages $\pi^{\leftarrow}(x, y, z)$ of a Cartesian point (x, y, z) are represented as follows. If $(y, z) = (0, 0)$ then we have $\|U\| \, \|V\| = 0$, and:

$$\pi^{\leftarrow}(x, 0, 0) = \left\{ \begin{array}{ll} \{u : \ u_1^2 + u_4^2 = X \ , \ u_2 = u_3 = 0\} & \text{for } X \geq 0 \\ \{u : \ u_2^2 + u_3^2 = -X \ , \ u_1 = u_4 = 0\} & \text{for } X < 0 \end{array} \right. \tag{47}$$

Instead, if $(y, z) \neq (0, 0)$, we first define $\beta \in [0, 2\pi)$ such that:

$$(y, z) = \sqrt{y^2 + z^2}(\cos\beta, \sin\beta),$$

[7] Consistently with the notations of the Introduction, we denote by $\Pi(x, y, z, \dot{x}, \dot{y}, \dot{z}) = (x, y, z)$ the projection from the Cartesian phase–space to the Cartesian configuration space.

and since $\|U\|^2 \|V\|^2 = (1/4)(y^2+z^2) \neq 0$, we introduce the polar representations

$$U = \|U\| (\cos\beta_U, \sin\beta_U) \quad , \quad V = \|V\| (\cos\beta_V, \sin\beta_V).$$

with well defined β_U, β_V (modulo 2π). From:

$$\begin{array}{rcl} X & = & \|U\|^2 - \|V\|^2 \\ y & = & 2\|U\|\|V\|\cos(\beta_U+\beta_V) \\ z & = & 2\|U\|\|V\|\sin(\beta_U+\beta_V), \end{array} \tag{48}$$

we obtain:

$$\pi^{\leftarrow}(x,y,z) = \{u : (u_1,u_4) = \frac{1}{\sqrt{2}}\sqrt{\sqrt{X^2+y^2+z^2}+X}\,(\cos\beta_U, \sin\beta_U) \quad ,$$

$$(u_2,u_3) = \frac{1}{\sqrt{2}}\sqrt{\sqrt{X^2+y^2+z^2}-X}\,(\cos(\beta-\beta_U), \sin(\beta-\beta_U)) \ , \beta_U \in [0,2\pi]\}. \tag{49}$$

From (47) and (49), we obtain that there exist α (dependent on x,y,z) such that $\tilde{u} = \mathcal{R}_\alpha u$. Now we consider $v, \tilde{v}$. From (16) we have:

$$(\dot{x},\dot{y},\dot{z},0) = \frac{2}{\|u\|^2}A(u)v = \frac{2}{\|\tilde{u}\|^2}A(\tilde{u})\tilde{v}$$

and since $\tilde{u} = \mathcal{R}_\alpha u$, we obtain[8]:

$$A(u)v = A(\mathcal{R}_\alpha u)\tilde{v} = A(\mathcal{R}_\alpha u)\mathcal{R}_\alpha\mathcal{R}_\alpha^T\tilde{v} = A(u)\mathcal{R}_\alpha^T\tilde{v}.$$

Therefore, we have $A(u)(v-\mathcal{R}_\alpha^T\tilde{v}) = 0$, and since $\Pi\mathcal{W} \subseteq \mathbb{R}_0^3$ and the matrix $A(u)$ is non-singular for $u \neq 0$, we obtain $\tilde{v} = \mathcal{R}_\alpha v$.

Let us now consider $\xi_0 \in \mathcal{W}$ and $\zeta_0 = \chi_1^{-1}(\xi_0)$, $\tilde{\zeta}_0 = \chi_2^{-1}(\xi_0) = R_\alpha\zeta_0$; denote by $\zeta(s)$ the solution of the regularized equations (27) with initial condition $\zeta(0) = \zeta_0$ and by $\tilde{\zeta}(s)$ the solution of the regularized equations (27) with initial condition $\tilde{\zeta}(0) = \tilde{\zeta}_0$. For any initial tangent vector $w(0)$, let us consider the solutions $w(s)$ of the variational equations defined by $\zeta(s)$. From the invariance properties (28) and (34) of the variational equation, $\tilde{w}(s) = R_\alpha w(s)$ is the solution of the variational equations for $\tilde{\zeta}(s)$ with initial conditions $R_\alpha w(0)$. Let us suppose that the maximum $\mathcal{F}$ on the right hand–side of (43), defined by using χ_1^{-1}, is obtained for a certain w_0; then since the integrand is invariant with respect to the rotations R_α of $\zeta(s)$ and $w(s)$, the maximum of the right hand–side of (43), defined by using χ_2^{-1}, is obtained for $\tilde{w}_0 = R_\alpha w_0$ and is equal to $\mathcal{F}$. This concludes the proof of the Lemma. □

To complete the proof of Theorem 1 we need to defined a covering of $\mathcal{M}_{C,T}$ with smooth local inversions.

Lemma 2. *The maps*

$$\pi_-^{-1} : \mathbb{R}^3 \backslash \{(x,0,0) : x \geq 1-\mu\} \longrightarrow \mathbb{U}$$

[8]The matrix $A(U)$ satisfies: $A(\mathcal{R}_\alpha u)\mathcal{R}_\alpha = A(u)$.

$$\pi_+^{-1} : \mathbb{R}^3 \backslash \{(x,0,0) : x \leq 1-\mu\} \longrightarrow \mathbb{U}$$

defined by

$$\pi_-^{-1}(x,y,z) = \left(\frac{y}{\sqrt{2(r-X)}}, \frac{\sqrt{r-X}}{\sqrt{2}}, 0, \frac{z}{\sqrt{2(r-X)}} \right)$$

$$\pi_+^{-1}(x,y,z) = \left(\frac{\sqrt{r+X}}{\sqrt{2}}, \frac{y}{\sqrt{2(r+X)}}, \frac{z}{\sqrt{2(r+X)}}, 0 \right),$$

where $X = x - 1 + \mu$ *and* $r = \sqrt{X^2+y^2+z^2}$*, are smooth and satisfy* $\pi \circ \pi_-^{-1}(x,y,z) = (x,y,z)$*,* $\pi \circ \pi_+^{-1}(x,y,z) = (x,y,z)$*.*

We define two local inversions χ_-^{-1}, χ_+^{-1} by extending the inverse maps π_-^{-1}, π_+^{-1} to the velocities:

$$\begin{array}{rcl} (u,v) = \chi_-^{-1}(x,y,z,\dot{x},\dot{y},\dot{z}) & = & (\pi_-^{-1}(x,y,z), \tilde{\pi}_-^{-1}(x,y,z,\dot{x},\dot{y},\dot{z})) \\ (u,v) = \chi_+^{-1}(x,y,z,\dot{x},\dot{y},\dot{z}) & = & (\pi_+^{-1}(x,y,z), \tilde{\pi}_+^{-1}(x,y,z,\dot{x},\dot{y},\dot{z})) \end{array} \tag{50}$$

with $\tilde{\pi}_-^{-1}, \tilde{\pi}_+^{-1}$ defined by:

$$\nu = \tilde{\pi}_\pm^{-1}(x,y,z,\dot{x},\dot{y},\dot{z}) = \frac{1}{2} A^T(\pi_\pm^{-1}(x,y,z))(\dot{x},\dot{y},\dot{z},0). \tag{51}$$

The proof of Theorem 1 is complete. □.

The computation of the maximum over all the tangent vectors of unitary norm in (43) is CPU-expensive. Therefore, it can be convenient to consider indicators defined by integrating single initial tangent vectors, in the spirit of the definition of Fast Lyapunov Indicators originally introduced in [7]. In the present case, the Fast Lyapunov Indicators will not be not globally defined on $\mathcal{M}_{C,T}$, therefore we need to consider at least two indicators defined using the two local inversions χ_-^{-1}, χ_+^{-1} respectively; the transition formula from the FLI defined with χ_-^{-1} to the FLI defined with χ_+^{-1} is provided below.

Definition 2. *For any positive time* $T > 0$*, for any* $\xi_0 = (x_0, y_0, z_0, \dot{x}_0, \dot{y}_0, \dot{z}_0) \in \mathcal{M}_C$ *and any* $w_0 \in \mathbb{R}^8$*, if* $(x_0,y_0,z_0) \in \mathbb{R}^3 \backslash \{(x,0,0) : x \leq 1-\mu\}$ *we define the modified fast Lyapunov indicator (mFLI hereafter) by:*

$$FLI_\phi^+(\xi_0, w_0, T) = \max_{t \in [0,T]} \int_0^{\sigma(\xi_0,t)} \phi(\mathcal{X}(\zeta_+(s)) \frac{w_+(s) \cdot w_+'(s)}{\|w_+(s)\|^2} ds, \tag{52}$$

while if $(x_0,y_0,z_0) \in \mathbb{R}^3 \backslash \{(x,0,0) : x > 1-\mu\}$ *we define the modified fast Lyapunov indicator (mFLI hereafter) by:*

$$FLI_\phi^-(\xi_0, w_0, T) = \max_{t \in [0,T]} \int_0^{\sigma(\xi_0,t)} \phi(\mathcal{X}(\zeta_-(s)) \frac{w_-(s) \cdot w_-'(s)}{\|w_-(s)\|^2} ds, \tag{53}$$

where $\zeta_\pm(s)$ are the solutions of equations (27) with initial conditions $\zeta_\pm(0) = \chi_\pm^{-1}(\xi_0)$; $w_\pm(s)$ is the solution of the variational equations (29) defined by $\zeta_\pm(s)$ with initial conditions $w_\pm(0) = w_0$ and $\sigma(\xi_0, t)$ denotes the the transformation $s := \sigma(\xi_0, t)$ between the physical time t and the proper time s for the orbit with initial condition ξ_0.

We remark that, for any fixed $w_0 \in \mathbb{R}^8$, and if $(y_0, z_0) \neq (0, 0)$, both indicators FLI_ϕ^-, FLI_ϕ^+ are defined, and the correspondence between them is:

$$FLI_\phi^+(\xi_0, w_0, T) = FLI_\phi^-(\xi_0, \mathcal{R}_\alpha w_0, T), \tag{54}$$

where α is defined by $\chi_-^{-1}(\xi_0) = R_\alpha \chi_+^{-1}(\xi_0)$. In fact, denoting by $\zeta(s), \tilde{\zeta}(s)$ the solutions of the regularized equations (27) with initial conditions $\zeta_0 = \chi_+^{-1}(\xi_0)$, $\tilde{\zeta}_0 = \chi_-^{-1}(\xi_0) = R_\alpha \zeta_0$ respectively, we have $\tilde{\zeta}(s) = R_\alpha \zeta(s)$. Moreover, if $w(s), \tilde{w}(s)$ are the the solutions of the variational equations for $\zeta(s), \tilde{\zeta}(s)$ with initial conditions $w_0, R_\alpha w_0$ respectively, we have $\tilde{w}(s) = R_\alpha w(s)$. Finally, the integrand in (52) and (53) is invariant with respect to the transformation $w(s) \to R_\alpha w(s)$. Instead, none of the two indicators $FLI_\phi^\pm(\cdot, w_0, T)$ has a smooth global extension to the sets $\mathcal{M}_{C,T}$ which are not completely contained in the domain of χ_+^{-1} or of χ_-^{-1}.

Remark 2. If instead of the finite time chaos indicators we consider the Lyapunov exponents defined using the regularized variational equations (29):

$$l_\pm(\xi_0, w_0) = \lim_{s \to +\infty} \frac{1}{s} \ln \|w_\pm(s)\|,$$

where $w_\pm(s)$ denote the solutions of (29) defined by the solutions $\zeta_\pm(s)$ of (27) with initial conditions $\zeta_\pm(0) = \chi_\pm^{-1}(\xi_0)$, we have:

$$l_+(\xi_0, w_0) = l_-(\xi_0, R_\alpha w_0)$$

where α is defined by $\chi_-^{-1}(\xi_0) = R_\alpha \chi_+^{-1}(\xi_0)$. Again, the largest Lyapunov exponent:

$$l(\xi_0) = \max_{w_0 \in \mathbb{R}^8 : \|w_0\| = 1} l_+(\xi_0, w_0) = \max_{w_0 \in \mathbb{R}^8 : \|w_0\| = 1} l_-(\xi_0, w_0)$$

is globally defined (if the limits converge to some real values), while the individual Lyapunov exponents $l_\pm(\cdot, w_0)$ are not.

Remark 3. In [12, 24] we defined modified FLIs by using the variational equations of the planar circular restricted three-body problem regularized with the Levi-Civita transformation:

$$\begin{cases} x &= 1 - \mu + u_1^2 - u_2^2 \\ y &= 2u_1 u_2 \end{cases} \tag{55}$$

and by the proper-time transformation $dt = r_2 ds$. For $(x, y) \neq (1 - \mu, 0)$ the LC transformation has two preimages (u_1, u_2) and $(-u_1, -u_2)$. Therefore, since the

Lyapunov exponents and the fast Lyapunov indicators are defined using norms of tangent vectors, they are globally defined. The geometric problem appears only for the KS transformation.

We finally comment the modification of the FTLE (43) and FLI (52),(53) by the introduction of the function $\phi(\mathcal{X}(\zeta(s))$ in the integrand which weights the contribution to the indicator of the solutions $w(s)$ of the variational equations. For the special choice

$$\phi(\xi) = 1 \quad \forall \xi \in \mathcal{M}_C,$$

the mFLI defined in (52),(53) become usual fast Lyapunov indicators (introduced in [7]), defined using the regularized variational equations (29):

$$FLI_{\phi}^{\pm}(\xi_0, w_0, T) = \max_{t\in[0,T]} \ln \frac{\|w_{\pm}(\sigma(\xi_0, t))\|}{\|w_0\|}, \tag{56}$$

and the mFTLE becomes:

$$\mathcal{F}_{\phi}^{T}(\xi_0) = \max_{t\in[0,T]} \max_{w} \ln \frac{\|w(\sigma(\xi_0, t))\|}{\|w(0)\|}, \tag{57}$$

(the quantity following the $\max_t$ being the usual finite time Lyapunov exponent introduced in [37], defined using the regularized variational equations (29)). Instead, when the weight function $\phi(\xi)$ is equal (or very close) to 1 in a small neighbourhood $\mathcal{U}_i$ of the center manifold $W^c_{C,i}$, and rapidly decays to zero outside $\mathcal{U}_i$, computations of the indicators $FLI_{\phi}^{\pm}$ and $\mathcal{F}_{\phi}^{T}$ provide sharp localization of the stable manifolds $W^s_{C,i}$ of $W^c_{C,i}$ (the unstable manifolds are obtained by computing the indicators for negative times T), as it will be explained in Section 4.

4 Hypertube manifolds computations with geometric chaos indicators

The ridges of finite time chaos indicators, such as the traditional FTLE and FLI originally defined in [37, 7], have been identified in the last decade as approximations of the stable and unstable manifolds of equilibria and periodic orbits, and the so called Lagrangian coherent structures of turbulent flows of many model systems (see for example [10, 11, 38, 22, 12, 31, 19, 20, 8]). In [13] we have shown that, depending on certain non-linear properties of the dynamical system, the traditional finite time chaos indicators can fail completely the detection of the stable or unstable manifolds of hyperbolic equilibria or periodic orbits. The problem has been solved by taking into account for the computation of the chaos indicator only the contributions from the variational equations due to a neighbourhood of the hyperbolic fixed point or periodic orbit. The method of [13] is here generalized to compute approximations of the stable manifolds of the center manifolds of L_1, L_2 as the ridges of modified finite time chaos indicators.

The discussion of this section remains valid, with small modifications, for the differential equations with a saddle-center-....-center equilibrium point (hypothesis (i)) and with a first integral with a quadratically non degenerate maximum or minimum when restricted to the center space of the equilibrium (hypothesis (ii))[9].

Several definitions of ridges for finite time chaos indicators have been given in the literature since [20, 31, 25], corresponding to the motivations related to the definition of the so called Lagrangian coherent structures. In this paper, the ridges of the chaos indicators are used with different purposes, for which we provide the following definition.

Definition 3. *Let us consider a two dimensional real function $F : \mathbb{R}^2 \to \mathbb{R}$. The smooth curve $\Gamma \in \mathbb{R}^2$ is a ridge of F if there exists a family of curves $\gamma_\eta(x)$ (x, defined in a neighbourhood of 0, is a parameter along the curve; η is defined in an interval) transverse to Γ at $\gamma_\eta(0)$, and such that $F(\gamma_\eta(x))$ has a strict absolute maximum at $x = 0$.*

Specifically, we will consider the ridges of the modified chaos indicators (43), (52), (53) restricted to two–dimensional surfaces $\Sigma \subseteq \mathcal{M}_C$ transverse to the stable manifolds $W^s_{C,i}$. We claim that for suitable choices of the neighbourhood $\mathcal{U}_i$, of the weight function $\phi(\xi)$ and, for the $FLI^{\pm}_{\phi}$ of the parameters w_0, the subset $W^s(T) \cap \Sigma$ of the stable manifolds defined by:

$$W^s(T) = \{\xi \in W^s_{C,i} : \quad \varphi(t,\xi) \in W^s_{C,loc} \ \ \forall\, t \geq T/2\}$$

where $\varphi(t,\xi)$ denotes the flow of the three-body problem in the Cartesian phase-space and

$$W^s_{C,loc} = \{\xi \in \mathcal{U}_i \cap W^s_{C,i} : \quad \varphi(t,\xi) \in \mathcal{U}_i \cap W^s_{C,i} \ \ \forall\, t \geq 0\}$$

denotes the local stable manifold in the set $\mathcal{U}_i$, is close to a ridge of the indicators $FLI^{\pm}_{\phi}(\xi, w_0, T), \mathcal{F}^T_{\phi}(\xi)$ restricted to Σ.

Let us continue our discussion by considering the case of L_1 (the case of L_2 can be obtained with very simple modifications) and by fixing the total time T and a value C of the Jacobi constant; we will assume, where needed, that $\varepsilon = C - C_1 > 0$ is suitably small. While in Definitions 1 and 2 (as well as in the applications of Section 6) the weight function $\phi(\xi)$ is smooth, in this Section we consider for simplicity a weight function $\phi(\xi)$ corresponding to the characteristic function of a suitably small neighbourhood $\mathcal{U}_i$ of $W^c_{C,i}$. Similar results are obtained for smooth weight functions whose value is 1 in the set $\mathcal{U}_i$, and outside $\mathcal{U}_i$ rapidly decay to zero, see Section 5. We consider two properties of the dynamics in the sets $\mathcal{U}_i$ which are valid with the above assumptions.

– *The scattering time from $\mathcal{U}_i$.* Any solution with initial conditions $\xi \in \mathcal{U}_i \backslash W^s_{C,loc}$ is scattered outside $\mathcal{U}_i$ in a finite time t_ξ (i.e. there exists a minimum $t_\xi > 0$ such that $\varphi(t_\xi, \xi) \notin \mathcal{U}_i$). The exit time t_ξ diverges at the local stable manifold.

[9] In particular, hypothesis (ii) cannot be removed, while hypothesis (i) could be relaxed to saddle-....-saddle-center-....-center cases, with some non-resonance condition on the eigenvalues.

– *Expansions of tangent vectors in* $\mathcal{U}_i$. For any ζ such that $\chi(\zeta) \in \mathcal{U}_i$, and any $s > 0$, we consider:

$$\lambda(s,\zeta) = \frac{1}{s} \ln \left\| \frac{\partial \tilde{\varphi}}{\partial \zeta}(s,\zeta) \right\| ,$$

where $\tilde{\varphi}(s,\zeta)$ denotes the flow of (27)[10] In the above hypotheses, $\lambda(s,\zeta)$ is continuous with respect to ζ; also, for any ζ such that $\chi(\zeta) \in \mathcal{U}_i$ and any $s \in [0, S(\zeta,T)]$ with:

$$S(\zeta,T) = \min\left(\sigma(\chi(\zeta),T), \sup\{s \geq 0 : \quad \chi(\tilde{\varphi}(s,\zeta)) \in \mathcal{U}_i\}\right) \quad ,$$

we have

$$0 < \lambda_\varepsilon^1 \leq \lambda(s,\zeta) \leq \lambda_\varepsilon^2$$

with $\lambda_\varepsilon^1, \lambda_\varepsilon^2$ constants depending only on ε (and the fixed T) and satisfying:

$$\lim_{\varepsilon \to 0} \lambda_\varepsilon^1 = \lim_{\varepsilon \to 0} \lambda_\varepsilon^2 = \lambda^\varepsilon, \tag{58}$$

with λ^ε defined in Subsection 2.4.

Below we provide estimates for $\mathcal{F}_\phi^T(\xi)$ in three different cases.

(i) Let us consider $\xi_0 \in W_C^s(T) \cap \Sigma$. Denote by $T_{\xi_0} < T/2$ the minimum time t such that $\varphi(\xi_0,t) \in \overline{W_{C,loc}^s}$, for any $t \in [T_{\xi_0}, T]$.

For any solution $\zeta(s)$ of equations (27) with $\chi(\zeta(s)) = \varphi(t(s),\xi_0)$ and any solution $w(s)$ of the variational equations (29) defined by $\zeta(s)$ with $w(0) = w_0$, we have:

$$\int_0^{\sigma(\xi_0,t)} \phi(\varphi(t(s),\xi_0)) \frac{w(s)\cdot w'(s)}{\|w(s)\|^2} ds = \ln \frac{\|w(\sigma(\xi_0,t))\|}{\|w(\sigma(\xi_0,T_{\xi_0}))\|} \ , \ \forall t \geq T_{\xi_0}. \tag{59}$$

Since $\tilde{\varphi}(s, \ \cdot \ )$ is a diffeomorphism, from (59) and (58) we obtain:

$$\begin{aligned}
\mathcal{F}_\phi^T(\xi_0) &= \max_{t\in[0,T]} \max_{w_0 \in \mathbb{R}^8, \|w_0\|=1} \textstyle\int_0^{\sigma(\xi_0,t)} \phi(\varphi(t(s),\xi_0)) \frac{w(s)\cdot w'(s)}{\|w(s)\|^2} ds = \\
&= \max_{t\in[0,T]} \max_{w_0 \in \mathbb{R}^8, \|w_0\|=1} \ln \left\| \tfrac{\partial \tilde{\varphi}}{\partial \zeta}(\sigma(\xi_0,t) - \sigma(\xi_0,T_{\xi_0}), \zeta(\sigma(\xi_0,T_{\xi_0})))w_0 \right\| \\
&= \max_{t\in[0,T]} \ln \left\| \tfrac{\partial \tilde{\varphi}}{\partial \zeta}(\sigma(\xi_0,t) - \sigma(\xi_0,T_{\xi_0}), \zeta(\sigma(\xi_0,T_{\xi_0}))) \right\| \\
&= \max_{t\in[0,T]} \Big(\sigma(\xi_0,t) - \sigma(\xi_0,T_{\xi_0})\Big) \lambda(\sigma(\xi_0,t), \zeta(\sigma(\xi_0,T_{\xi_0}))) \\
&\in \Big(\sigma(\xi_0,T) - \sigma(\xi_0,T_{\xi_0})\Big) [\lambda_\varepsilon^1, \lambda_\varepsilon^2].
\end{aligned} \tag{60}$$

(ii) Let us consider $\xi \notin W_C^s(T)$, but very close to ξ_0. Denote by T_ξ the minimum time such that $\varphi(t,\xi) \in \overline{\mathcal{U}}_i$. For any solution $\zeta(s)$ of equations (27) with $\chi(\zeta(s)) = \varphi(t(s),\xi)$ we denote by $w(s)$ the solution of the variational equations (29) defined by $\zeta(s)$ with $w(0) = w_0$. From standard Lipschitz estimates we have that T_ξ

[10]The norm of the Jacobian matrix is the matrix norm: $\|B\| = \max_{V:\|V\|=1} \|BV\|$.

is close to T_{ξ_0}, and for suitably small $\|\xi-\xi_0\|$, we have $\varphi(t,\xi)\in\mathcal{U}_i$ for any $t\in[T_\xi,T]$. The estimate of the FTLE is therefore

$$\begin{aligned}\mathcal{F}_\phi^T(\xi)&=\max_{t\in[0,T]}\max_{w_0\in\mathbb{R}^8,\|w_0\|=1}\int_0^{\sigma(\xi,t)}\phi(\varphi(t(s),\xi))\tfrac{w(s)\cdot w'(s)}{\|w(s)\|^2}ds=\\&=\max_{t\in[0,T]}\ln\left\|\tfrac{\partial\tilde\varphi}{\partial\zeta}(\sigma(\xi,t)-\sigma(\xi,T_\xi),\zeta(\sigma(\xi,T_\xi)))\right\|\\&=\max_{t\in[0,T]}\Big(\sigma(\xi,t)-\sigma(\xi,T_\xi)\Big)\lambda(\sigma(\xi,t),\zeta(\sigma(\xi,T_\xi)))\\&\in\Big(\sigma(\xi,T)-\sigma(\xi,T_\xi)\Big)[\lambda_\varepsilon^1,\lambda_\varepsilon^2].\end{aligned}\tag{61}$$

(iii) Let us consider again $\xi\notin W_C^s(T)$ so close to ξ_0 that T_ξ is close to T_{ξ_0} (as in case (ii)), but now assume that the scattering time $t_{\varphi(T_\xi,\xi)}$ of $\varphi(T_\xi,\xi)$ satisfies:

$$t_{\varphi(T_\xi,\xi)}\le T-T_{\xi_0},$$

so that in the time interval $[T_\xi,T]$ the solution $\varphi(t,\xi)$ exits from $\mathcal{U}_i$. We consider the sequence of intervals for the proper time s:

$$I_1=(a_1,b_1),\ I_2=(a_2,b_2),\dots,I_{M_\xi}=(a_{M_\xi},b_{M_\xi})\subseteq[\sigma(T_\xi,\xi),\sigma(T,\xi)]$$

defined by $a_1<b_1\le a_2<b_2\le\ldots<b_{M_\xi}$ such that $\chi(\zeta(s))\in\mathcal{U}_i$ if and only if $s\in\cup I_j$. We have

$$\begin{aligned}\mathcal{F}_\phi^T(\xi)&=\max_{t\in[0,T]}\max_{w_0\in\mathbb{R}^8,\|w_0\|=1}\int_0^{\sigma(\xi,t)}\phi(\varphi(t(s),\xi))\tfrac{w(s)\cdot w'(s)}{\|w(s)\|^2}ds=\\&\le\textstyle\sum_{j=1}^{M_\xi}\left|\ln\left\|\tfrac{\partial\tilde\varphi}{\partial\zeta}(b_j-a_j,\zeta(a_j))\right\|\right|\\&\le\textstyle\sum_{j=1}^{M_\xi}(b_j-a_j)\lambda(b_j-a_j,\tfrac{\partial\tilde\varphi}{\partial\zeta}(b_j-a_j,\zeta(a_j)))\\&\in\textstyle\sum_{j=1}^{M_\xi}(b_j-a_j)[\lambda_\varepsilon^1,\lambda_\varepsilon^2].\end{aligned}\tag{62}$$

It remains to construct a a family of curves $\gamma_\eta(x)\in\Sigma$ which identifies a ridge $\Gamma\subseteq\Sigma$ for $\mathcal{F}_\phi^T$ in the section Σ, and to show that, using estimates (60), (61) and (62), the ridge is pointwise close to a given curve $\Gamma_0\subseteq W^s(T)\cap\Sigma$.

Under mild transversality conditions between Σ and $W^s(T)$, using a finite reduction to the center manifold defined in [14, 15] (see also Section 5), we construct a family of curves $\gamma_\eta(x)$ such that $\gamma_\eta(0)\in\Gamma_0$ and by considering $\tilde\gamma_\eta(x)=\varphi(T_{\gamma_\eta(x)},\gamma_\eta(x))$, if $t_{\tilde\gamma_\eta(x)}\le T$ it satisfies:

$$\frac{1}{\lambda_{L_1}+X\sqrt{\varepsilon}}\ln\frac{X\sqrt{\varepsilon}}{|x|}-\alpha_1\le t_{\tilde\gamma(\eta,x)}\le\frac{1}{\lambda_{L_1}-X\sqrt{\varepsilon}}\ln\frac{X\sqrt{\varepsilon}}{|x|}+\alpha_1\tag{63}$$

with α_1,X positive constants not depending on ε,x. From inequalities (63) we find a neighbourhood $\mathcal{I}_0$ of $x=0$ such that $\gamma_\eta(x)$ is as in case (ii), and therefore $\mathcal{F}_\phi^T(\gamma_\eta(x))$ is close to $\mathcal{F}_\phi^T(\gamma_\eta(0))$; we also find a neighbourhood $\mathcal{I}_1\supset\mathcal{I}_0$ of $x=0$ such that, for $x\in\mathcal{I}_1\backslash\mathcal{I}_0$, $\gamma_\eta(x)$ are as in case (iii) with $M_\xi=1$. In particular, for $x\in\mathcal{I}_1\backslash\mathcal{I}_0$, we have:

$$\mathcal{F}_\phi^T(\gamma_\eta(0))\ge\mathcal{F}_\phi^T(\gamma_\eta(x))+[\sigma(\xi_0,T)-\sigma(\xi_0,T_{\gamma_\eta(x)})-\sigma(\gamma_\eta(x),t_{\tilde\gamma_\eta(x)})]\lambda_\varepsilon^1+\ldots.$$

where the dots means terms which are as small as ε and $|x|$. Therefore, the ridge defined by the absolute maxima of $\mathcal{F}_\phi^T(\gamma(\eta, x))$ is contained a a smaller neighbourhood of $x = 0$, strictly contained in $\mathcal{I}_1$. A riparametrization of the curves $\gamma_\eta(x)$ which moves the origin of the parameter to the absolute maximum of the FTLE completes the construction of the family of curves identifying the ridge Γ.

Remark 4. The logarithmic dependence of the scattering time (63) from x makes the distance between the ridge Γ and the curve $\Gamma_0 \subseteq W^s(T)$ extremely small. Precisely, we have a linear decrement of the mFTLE with respect to $\ln|x|$, up to the maximum value of a quantity proportional to $T - T_\xi - t_{\tilde{\gamma}_\eta(x)} \leq T - T_{\xi_0}$; differences of units in the mFTLE value typically determine a proportional number of precision digits in the localization of the stable manifold.

Remark 5. If the curve Γ_0 is completely contained in the domain of the local inversions χ_+^{-1} or χ_-^{-1}, with a very mild assumption of the initial tangent vector w_0, the curve Γ_0 is close to a ridge of FLI_ϕ^+ or FLI_ϕ^-, defined by w_0. In fact, by excluding a linear subspace of $\mathbb{R}^8$, all the initial tangent vectors are expanded exponentially at rates between $\lambda_\varepsilon^1, \lambda_\varepsilon^2$.

5 Definition of the weight function $\phi(\xi)$

To compute the chaos indicators defined in Section 3, having the properties discussed in Section 4, we need to define explicitly a weight functions $\phi(\xi)$ whose values are equal to 1 very close to the center manifold $W_{C,i}^c$, and then decay rapidly to zero when the distance between ξ and the center manifold of L_i is larger than a fixed small radius ρ.

It is not sustainable, from a computational point of view, to define $\phi(\xi)$ as a function of the minimum distance between ξ and a refined grid of points on the selected center manifold $W_{C,i}^c$. In fact, this would require to construct a grid of the same dimension as $W_{C,i}^c$ of step-size smaller than ρ and to compute the distance of ξ from all the points of the grid. Then, to compute the integrals defining the modified chaos indicators, such an operation must repeated thousands of times. As a matter of fact, the geometry of the phase-space close to $W_{C,i}^c$ allows us to define ϕ in a more efficient way.

At this purpose, we consider a finite order approximation of $W_{C,i}^c$ provided by the so called Hamiltonian reductions to the center manifold (see [14, 15]). Precisely, for any integer N, we explicitly construct canonical variables p, q defined in a neighbourhood of the origin (identified with L_1 or L_2), giving the Hamiltonian of the spatial circular restricted three-body problem the form:

$$H = \lambda p_1 q_1 + \omega_1 \frac{p_2^2 + q_2^2}{2} + \omega_2 \frac{p_3^2 + q_3^2}{2} + K(p, q) + R(p, q), \tag{64}$$

where K depends on p_1, q_1 only through the product $p_1 q_1$ and is at least of order 3 with respect to p, q and R is a remainder of order N. The finite order

approximations of the center manifold are obtained by setting $R = 0$ in the Hamiltonian (64): for the truncated Hamiltonian, the equations $p_1, q_1 = 0$ define the center manifold, the equation $q_1 = 0$ its local stable manifold, the equation $p_1 = 0$ its local unstable manifold, the action $p_1 q_1$ is a constant of motion. The construction of the variables p, q is explicit, and is achieved through $N - 2$ hyperbolic Birkhoff steps (see [14, 15]).

Using the variables p, q we define a neighbourhood $\mathcal{U}_i$ ($i = 1$ for L_1, $i = 2$ for L_2) of the center manifold in $\mathcal{M}_C$. By denoting with

$$(q, p) := (q(\xi), p(\xi))$$

the transformation from the Cartesian phase-space variables to the (q, p), we consider the set:

$$\mathcal{U}_i = \{\xi \in \mathcal{M}_C : \quad |q_1(\xi)|, |p_1(\xi)| < \rho\}.$$

Since for the truncated Hamiltonian the center manifold is defined by $p_1(\xi), q_1(\xi) = 0$, for the complete Hamiltonian system (64) (and therefore for the exact three-body problem) if ρ is not too small the set $\mathcal{U}_i$ remains a neighbourhood of the center manifold.

In principle, one could think to work with the highest possible truncation order N allowed by a certain value of the Jacobi constant C. This is not necessary, and also not convenient. In fact, on the one hand, we do not need the manifold to correspond exactly to the center of the neighbourhood $\mathcal{U}$; on the other hand, since the variables q, p are explicitly constructed as the sum of polynomials of maximum order $N - 1$ of the 6 Cartesian variables ξ_i, the numerical cost for their computation increases rapidly with N. We therefore have chosen $N = 5$, and found no differences in the numerical computation of the stable-unstable manifolds with respect to $N = 6$. The variables are constructed by implementing only 2 Birkhoff normalization steps, as described in the paper [15], and by truncating the series expansions at order 4. Then, the weight function is defined by:

$$\phi(\xi) = \begin{cases} 1 & \text{if} \quad \rho(\xi) \leq \frac{\rho}{2} \\ \frac{1}{2}[\cos((\frac{\rho(\xi)}{\rho} - \frac{1}{2})\pi) + 1] & \text{if} \quad \frac{\rho}{2} < \rho(\xi) \leq \frac{3r}{2} \\ 0 & \text{if} \quad \rho(\xi) > \frac{3\rho}{2} \end{cases} . \tag{65}$$

where $\rho(\xi) = \sqrt{q_1(\xi)^2 + p_1(\xi)^2}$.

In particular, we have $\phi(\xi) = 1$ for $\rho(\xi) \leq \rho/2$, and $\phi(\xi)$ decays to 0 at $\rho(\xi) = 3\rho/2$. Since $\phi(\xi)$ is smooth, from Theorem 1 also the chaos indicator $\mathcal{F}_\phi^T$ is smooth, as well as the indicators FLI_ϕ^+, FLI_ϕ^- in the domains of χ_+^{-1}, χ_-^{-1} respectively. In Section 6 we will also identify with $\phi_1(\xi)$ and $\phi_2(\xi)$ the weight functions (65) defined using the reductions to the center manifolds of L_1 and L_2 respectively.

6 Application to the Sun-Jupiter case

In this section we represent the intersections of the stable manifolds $W^s_{C,1}, W^s_{C,2}$ of the center manifolds $W^c_{C,1}, W^c_{C,2}$ of L_1, L_2 with the planar section Σ_P and the vertical section Σ_V, defined in (3) and (4), computed as the ridges of the chaos indicators defined in Sections 3,4 and 5. As a model problem we consider the spatial three-body problem defined by the Sun-Jupiter masses and the value:

$$C = 3.0368573364394607$$

of the Jacobi constant, which is slightly smaller than C_2. Sections of the realms S, J, E as well as of the isolating blocks R_1, R_2 for such value have been represented in figure 1.

6.1 The planar section of the stable hypertube manifolds

The planar section Σ_P of the spatial circular restricted three-body problem is a subset of the reduced phase-space of the planar problem:

$$\mathcal{M}_P = \{(x, y, z, \dot{x}, \dot{y}, \dot{z}) : z = 0, \dot{z} = 0\}.$$

The sets $W^c_{C,1} \cap \mathcal{M}_P, W^c_{C,2} \cap \mathcal{M}_P$ contain only a planar Lyapunov periodic orbit, which we denote by LL_1, LL_2 respectively; the manifolds $W^s_{C,1} \cap \mathcal{M}_P$, $W^s_{C,2} \cap \mathcal{M}_P$ are the tubes of orbits converging to LL_1, LL_2. Intersections of the tube manifolds with the planar section have been provided in [13, 24]; in this subsection we reconsider the planar problem to support the interpretation of the results of the genuine spatial problem; in fact, the connected components of the intersections of the hypertube manifolds $W^s_{C,1}, W^s_{C,2}$ with the vertical section Σ_V are continuations of planar homoclinic orbits; moreover, different components which are disconnected in Σ_V, are connected in $\mathcal{M}_C$ through paths contained in the planar section, specifically paths of $W^s_{C,1} \cap \Sigma_P, W^s_{C,2} \cap \Sigma_P$.

In the top panel of figure 2 we report the ridges of the mFLI on the section Σ_P, computed using a weight function $\phi(\xi)$ which is different from zero only in a small neighbourhood of LL_1; in the realm J we have 4 ridges, which we denote by $\lambda^1_1, \ldots, \lambda^1_4$. The ridge λ^1_1, intersects LL_1 and extends on both sides of the Lyapunov orbit; all the orbits with initial conditions on λ^1_1 converge directly to LL_1 without performing circulations around P_1, P_2. The dynamics of orbits with initial conditions on $\lambda^1_2, \ldots, \lambda^1_4$ is more complicate. Let us consider the tube of orbits generated by the flow of the three-body problem with initial conditions on λ^1_2 (the red curve in the top panel of figure 2), represented in figure 3. The orbits obtained by integrating the initial conditions on λ^1_2 forward in time perform half circulation around P_2 and then intersect the section Σ_P at some point of λ^1_1 (see figure 3, top panel); then, as all the orbits with initial conditions on λ^1_1, they converge directly to LL_1. The tube of orbits obtained by integrating the initial conditions on λ^1_2 backward in time, after half a circulation of P_2, is so stretched

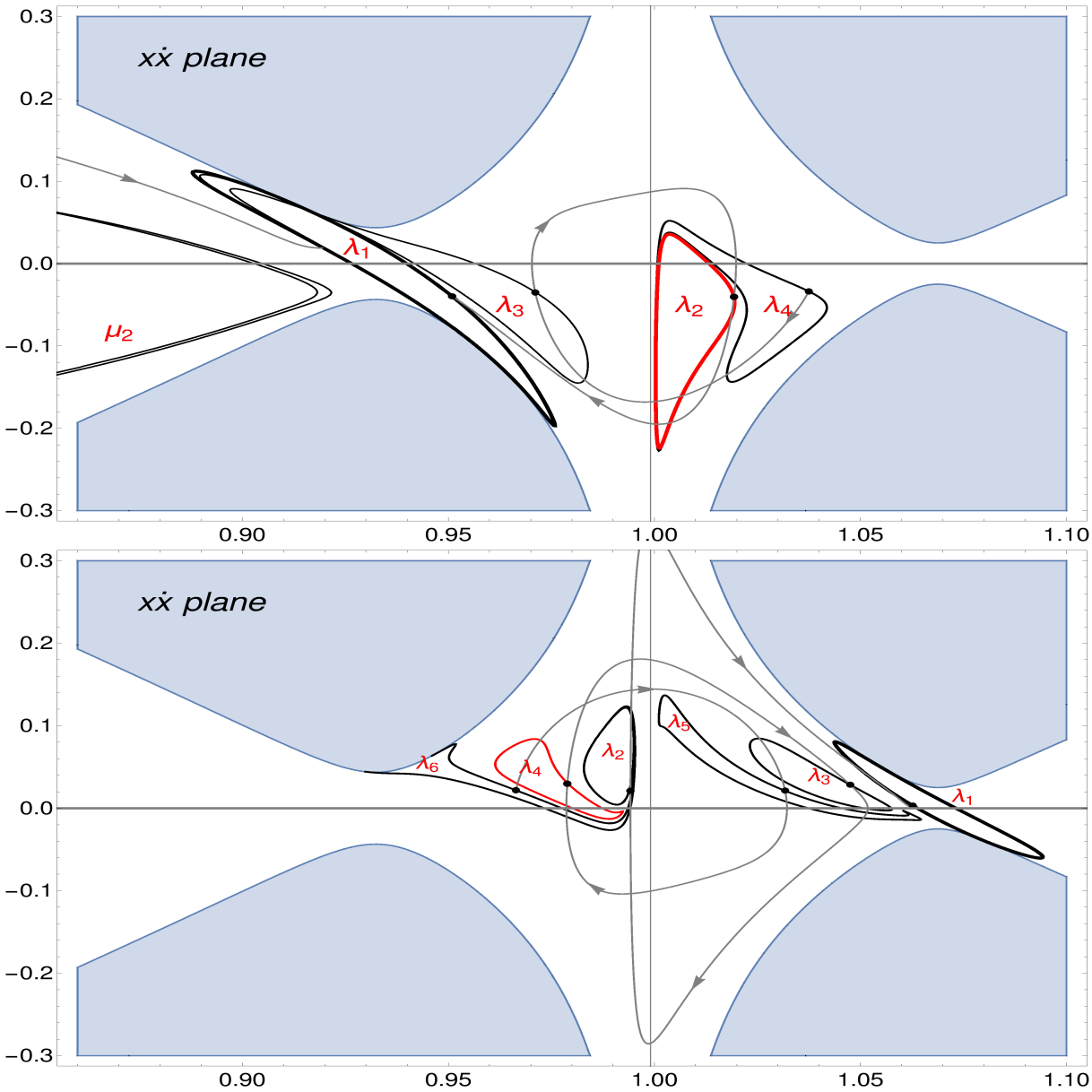

Figure 2: **Intersection of $W^s_{C,1}, W^s_{C,2}$ with the planar section Σ_P.** We represent the ridges of the mFLI on the vertical section Σ_P, parameterized by $x, \dot{x}$. The modulus $|\dot{y}|$ is obtained from the value of the Jacobi constant. In the top panel we represent the ridges $\mu^1_1, \lambda^1_1, \ldots, \lambda^1_4$ (the superscript is omitted in the figure) which approximate $W^s_{C,1} \cap \Sigma_P$. The curves λ^1_2, λ^2_4 are ridges of FLI^+_ϕ, while the other curves are ridges of FLI^-_ϕ; all the points of $\mu^1_2, \lambda^1_2, \lambda^1_4$ are characterized by $\dot{y} > 0$, while λ^1_1, λ^1_3 contain points with $\dot{y} \geq 0$ and $\dot{y} < 0$. In the bottom panel we represent the ridges $\lambda^2_1, \ldots, \lambda^2_6$ (the superscript is omitted in the figure) which approximate $W^s_{C,2} \cap \Sigma_P$. The curves $\lambda^2_1, \lambda^2_3, \lambda^2_5$ are the ridges of FLI^+_ϕ, while the other curves are ridges of FLI^-_ϕ; all the points of λ^2_3, λ^2_5 are characterized by $\dot{y} > 0$, $\lambda^2_2, \lambda^2_4, \lambda^2_6$ by $\dot{y} < 0$, while λ^1_1 contains points with $\dot{y} \geq 0$ and $\dot{y} < 0$. The gray curves represent the projection on Σ_P of two orbits with initial conditions on $W^s_{C,1}, W^s_{C,2}$ respectively; the orbits return to the section several times, intersecting different connected ridges on the points marked with a black bullet.

that a part transits directly to the realm of motions S without intersecting Σ_P; another part transits to the realm of motions S after two intersections with λ_3^1 (one with positive and one with negative $\dot{y}$); another part performs a circulation around P_2 intersecting Σ_V in a point of λ_3^1 and a point of λ_4^1. In particular, there are orbits tangent to the section Σ_P, determining such bifurcations in the transit properties. The possible transitions are summarized in figure 4, top panel; by extending the computations of the ridges to longer integration times we would detect additional ridges λ_i^1 and additional transitions. The topology of the manifold $W^s_{C,1}$ in the realm S (described in [24]) develops like a strip which folds in the interior realm S filling a large portion of S.

In the bottom panel of figure 2 we report the ridges of the mFLI on the section Σ_P, computed using a weight function $\phi(\xi)$ which is different from zero only in a small neighbourhood of LL_2; in the realm J we find six ridges, which we denote by $\lambda_1^2, \ldots, \lambda_6^2$. The ridge λ_1^2 intersects LL_2 and extends on both sides of the Lyapunov orbit; all the orbits with initial conditions on λ_1^2 converge directly to LL_2 without performing circulations around P_1, P_2. The tube of orbits generated by the forward-time flow of the three-body problem with initial conditions on λ_4^2 (the red curve in the bottom panel of 2) performs a full circulation of P_2, and intersects the section Σ_P at λ_3^2, λ_2^2 (see figure 5, top panel); then, the orbits with initial conditions on λ_2^2 perform an additional half circulation around P_2 and then intersect the section Σ_P at some point of λ_1^2; afterwards, as all the orbits with initial conditions on λ_1^2, they converge directly to LL_2. Then, we consider the tube of orbits generated by the backward-time flow with initial conditions on λ_4^2. Again, the tube perform half a circulation around P_2 till it intersects Σ_P in λ_5^2; then by continuing the backward integration of orbits with initial conditions on λ_5^2 we have three different possibilities: the orbit intersect Σ_P at λ_6^2, or they transit to the external realm E, or they transit to the internal realm S. The possible transitions are summarized in figure 4, bottom panel.

6.2 The vertical section of the hypertube manifolds

In the figures 6 and 7 we report the ridges of the mFLI on the section Σ_V, computed using both the weight functions $\phi_1(\xi), \phi_2(\xi)$ defined in Section 5. For $x > 1-\mu$ we report the ridges of the $FLI^+_{\phi_i}$ indicator, while for $x < 1-\mu$ we report the ridges of the $FLI^-_{\phi_i}$ indicator: since all the ridges do not cross the line $x = 1-\mu$, we are allowed to use the two modified FLI in place of the more CPU expensive modified FTLE.

The black curves are ridges of $FLI^{\pm}_{\phi_1}$: the bold black curve, which we denote by Λ_1^1, represents the intersection of the center manifold $W^c_{C,1}$ with the vertical section Σ_V; the other ridges represent intersections $W^s_{C,1} \cap \Sigma_V$. Two of these curves, which we denote by M_1^1, M_2^1, belong to the left hand side branch of the

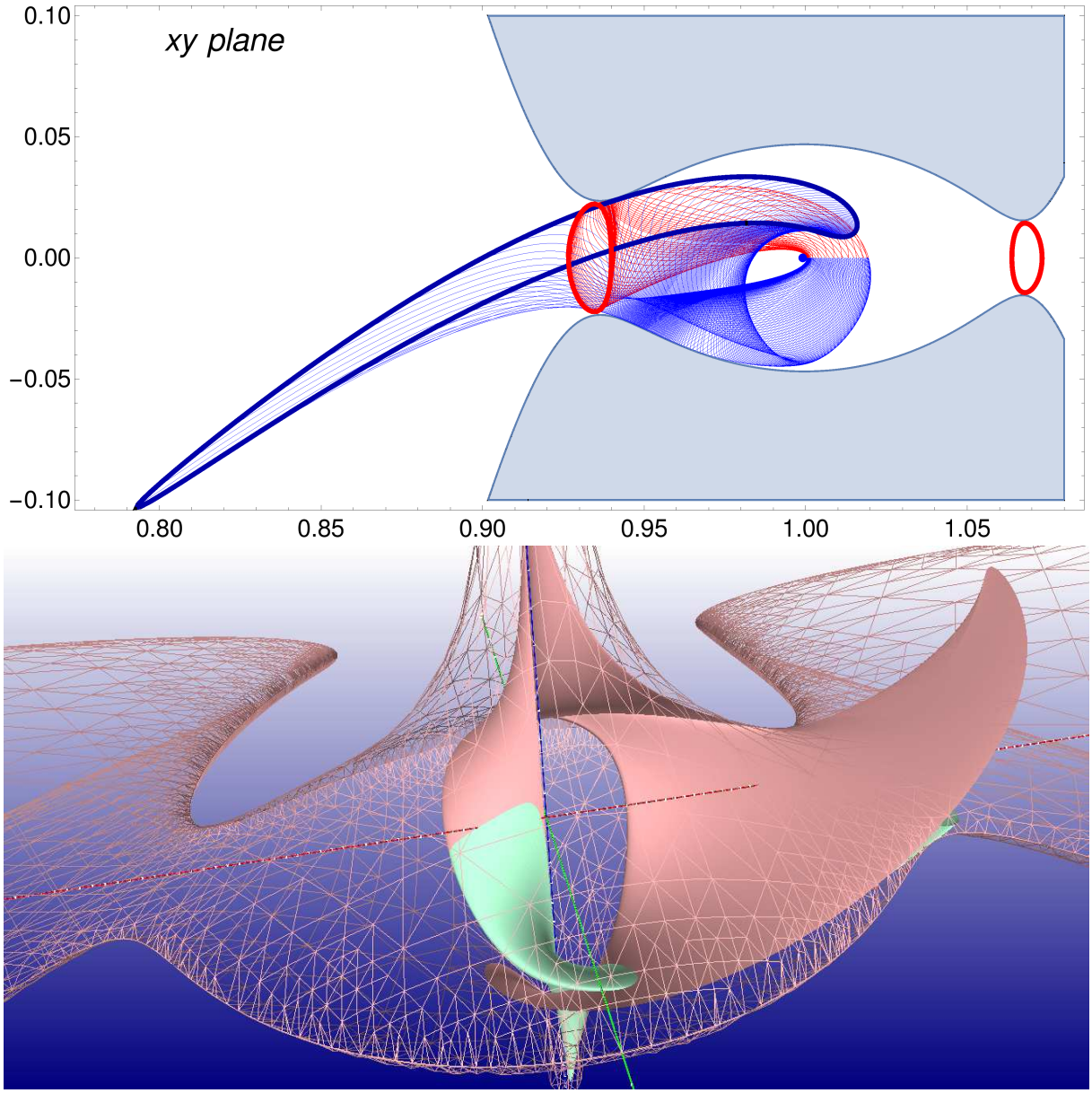

Figure 3: **Tube of orbits generated by** λ_2^1 obtained by integrating a sample of initial conditions both for positive and negative times. On the top panel we represent the projection of these orbits on the x, y plane. The red curves represent the orbits integrated for positive times; the blue curves represent the orbits integrated up to the negative proper time $s = -45$. The bold blue curve represents the border of the tube at $s = -45$. In the bottom panel we represent the tubes generated by the same orbits in the three-dimensional phase-space $x, y, \dot{x}$; a transparent mesh samples the border of $\mathcal{M}_C$. The light-green surface is the portion of stable–manifold obtained by integrating forward the initial conditions on λ_2^1, the pink surface represents the tube obtained by integrating backward the initial conditions on λ_2. The perspective is reversed with respect to the upper panel: the positive x axis points toward the left.

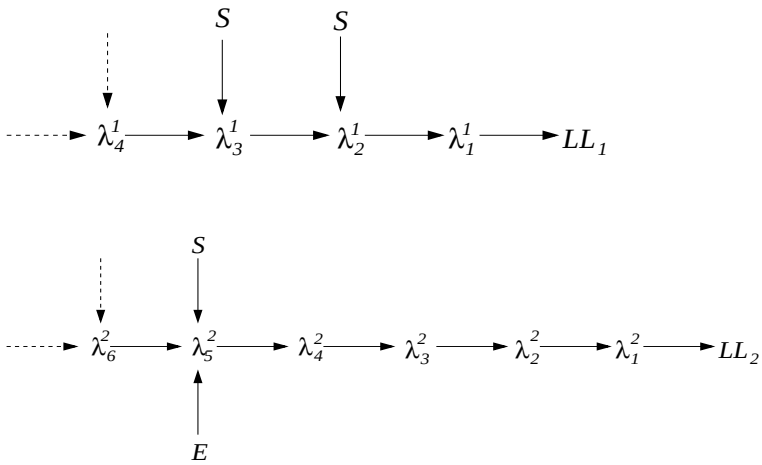

Figure 4: **Transitions between the curves λ_j^i and the realms J and S.** In the top panel we summarize the transition properties for the orbits with initial conditions on λ_i^1. The forward time evolution is simple: any initial conditions in λ_i^1 will intersect the section in $\lambda_{i-1}^1, \ldots, \lambda_1^1$ and then converges to LL_1. The backward time evolution has bifurcations, summarized by the diagram. In the bottom panel we summarize the transition properties for the orbits with initial conditions on λ_i^2. The forward time evolution is simple: any initial conditions in λ_i^2 will intersect the section in $\lambda_{i-1}^2, \ldots, \lambda_1^2$ and then converges to LL_2. The backward time evolution has bifurcations, summarized by the diagram.

stable manifold (see figure 7) and are in the realm S: the initial conditions on M_1^1 (which is on the right of the primary body) perform half of a circulation around the primary body before approaching the center manifold; the initial conditions on M_2^1 (which is on the left of the primary body) perform a complete circulation around the primary body before approaching the center manifold. The remaining curves (light black curves in figure 6) are on the right hand-side branch of the stable manifold, and we denote them by $\Lambda_2^1, \Lambda_3^1, \ldots, \Lambda_7^1$; where the lower index j labels the number $(j-1)/2$ of circulations around the secondary body before entering permanently the region R_1. These ridges intersect the corresponding planar ridges λ_j^1 (reported in figure 2, top panel) at the one dimensional section:

$$\Sigma_{VP} = \{(x, y, z, \dot{x}, \dot{y}, \dot{z}) : y = z = 0, \dot{x} = \dot{z} = 0, \mathcal{C}(x, 0, 0, \dot{y}, 0) = C\}. \qquad (66)$$

As a matter of fact, we found two disconnected ridges $\Lambda_4^1, \tilde{\Lambda}_4^1$ such that the orbits with initial conditions on both of them perform 3/2 circulations around P_2 before entering permanently the region R_1, see the bottom panels of figure 6. These two curves are disconnected in Σ_V but are connected in the phase-space $\mathcal{M}_C$ through the intersection $W_{C,1}^s \cap \Sigma_P$ of the stable manifold with the planar section, see figure 8. Such connections are expected to exist also for other ridges, and are important to determine the transit properties of the orbits with initial conditions on Σ_V, see Subsection 6.3.

The blue curves are ridges of $FLI_{\phi_2}^{\pm}$: the bold blue curve, which we denote by Λ_1^2, represents the intersection of the center manifold $W_{C,2}^c$ with the vertical

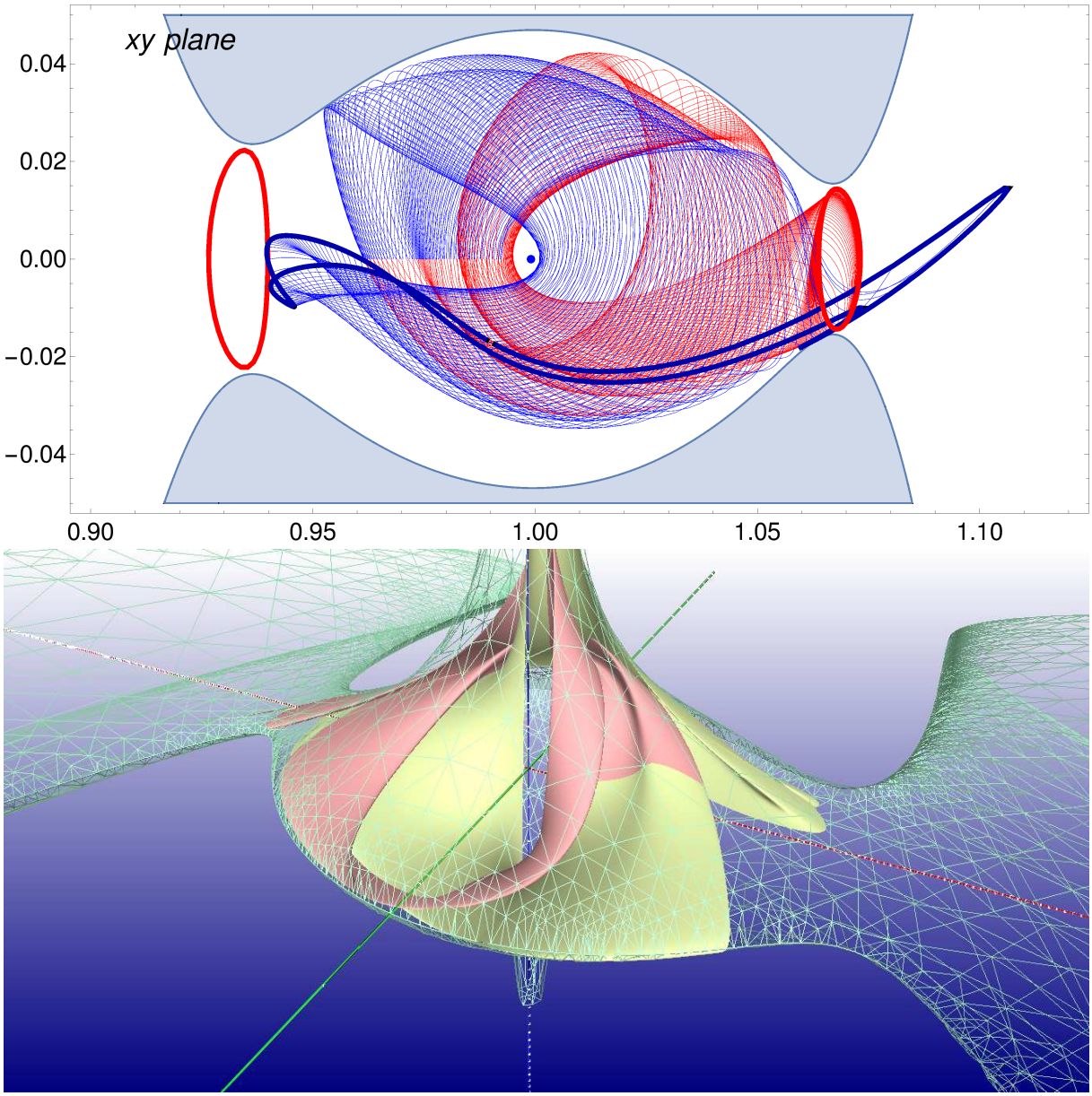

Figure 5: **Tube of orbits generated by** λ_4^2 obtained by integrating a sample of initial conditions both for positive and negative times. On the top panel we represent the projection of these orbits on the x, y plane. The red curves represent the orbits integrated for positive times; the blue curves represent the orbits integrated for negative times. The bold blue curve represents the border of the tube. In the bottom panel we represent the tubes generated by the same orbits in the three-dimensional phase-space $x, y, \dot{x}$; a transparent mesh samples the border of $\mathcal{M}_C$. The light-green surface is the portion of stable–manifold obtained by integrating backward the initial conditions on λ_4^2, the pink surface represents the tube obtained by integrating forward the initial conditions on λ_4^2. The perspective is reversed with respect to the upper panel: the positive x axis points toward the left.

section Σ_V, while the other ridges of $FLI^{\pm}_{\phi_2}$ (light blue curves in figure 6) are in the right left-hand side branch of the stable manifold $W^s_{C,2} \cap \Sigma_V$. We denote them by $\Lambda^2_3, \ldots, \lambda^2_7$, where the lower index j labels the number $(j-1)/2$ of circulations around the secondary body before entering permanently R_2 (see figure 1). These ridges intersect at Σ_{VP} the corresponding planar ridge λ^2_j reported in figure 2, bottom panel.

Methods of grids computation. The ridges represented in this paper are computed as an ordered sequence of close points $\pi_0, \pi_1, \ldots$. Since the sections Σ_V and Σ_P intersect at the one dimensional section Σ_{VP}, we preliminary compute the modified FLI for a grid of initial conditions on Σ_{VP}. Each maximum of the FLI on this one dimensional grid is close to a ridge of the FLI. Precisely, we select a point $\tilde{\pi}_0$ corresponding to one of these maxima, and we compute again the modified FLI on a much more refined one-dimensional grid centered in $\tilde{\pi}_0$. The maximum FLI on this new grid provides a better estimate of the the first point π_0 on the ridge of the FLI. The second point π_1 of the ridge is obtained by computing the FLI on another one-dimensional grid of points on Σ_V characterized by a small value ε_0 of the coordinate z, and the same coordinates $x, y, \dot{x}, \dot{z}$ of π_0; the value of $|\dot{y}|$ is determined from the value of the Jacobi constant. The maximum FLI on this second grid provides π_1. The third point π_2 is computed from a one-dimensional grid of N points chosen on an segment which is orthogonal to $\pi_1 - \pi_0$, whose center is at a distance ε_0 from π_1, and whose amplitude is equal to another small parameter ε_1. The maximum FLI on this grid provides the point π_2. The procedure is then iterated, providing an ordered set of points on a curve which samples a ridge of the mFLI with maximum error ε_1/N. The values of the parameters $\varepsilon_0, \varepsilon_1, N$ are adjusted at each step. Then, we select a subset of points π_i, and we refine the computation by recomputing the FLI on one dimensional grids centered on π_i, orthogonal to $\pi_i - \pi_{i-1}$, and with a new value for ε_1 which is set equal to $\varepsilon_1/2$. After K of these refinements, we obtain an ordered set of points on a curve which samples a ridge of the mFLI with maximum error $\varepsilon_1/(2^K N)$. After few iterations K of this process we arrive a the limit of the double precision floating point arithmetics (to reach the double precision in the computation of the manifold we perform the last steps of the iteration with the extended precision floating point arithmetics).

The equations of motion (27) and their variational equations (29) are numerically integrated with an explicit Runge-Kutta integration scheme of order six using double or extended floating point precision.

6.3 Survey of the dynamics in the section Σ_V

In this section we represent the dynamics of the orbits with initial conditions in the section Σ_V, with particular attention to the orbits with initial conditions

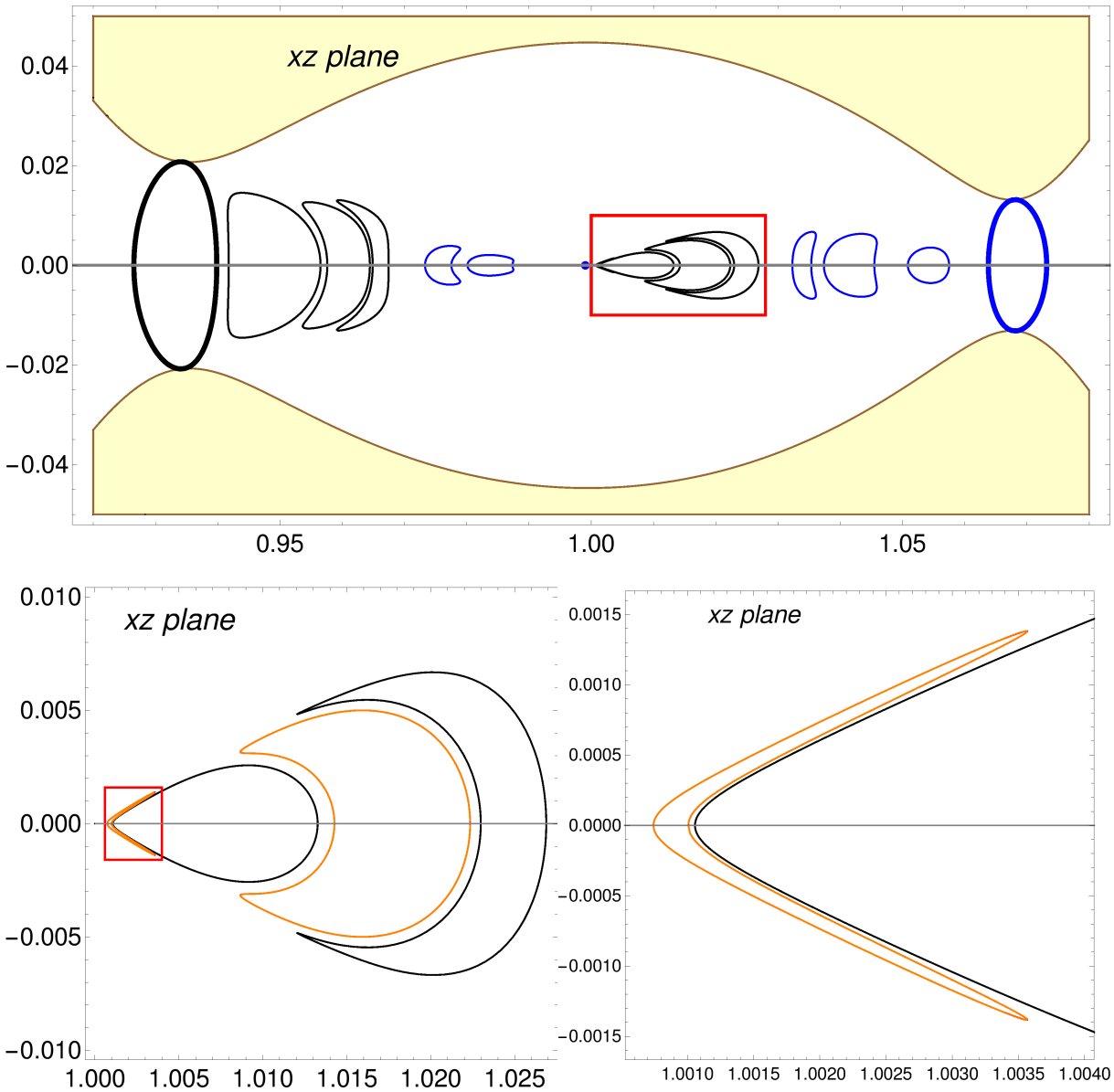

Figure 6: **Intersection of $W^s_{C,1}$ with the vertical section Σ_V in the realm J.** We represent the ridges of the mFLI on the vertical section Σ_V, parameterized by x, z. The modulus $|\dot{y}|$ is obtained from the value of the Jacobi constant; the other initial conditions are $y, \dot{x}, \dot{z} = 0$. The black curves have been obtained from $FLI^{\pm}_{\phi_1}$: the bold black curve Λ^1_1 represents $W^c_{C,1} \cap \Sigma_V$, the light black curves represent the $\Lambda^1_2, \ldots, \Lambda^1_7$. The blue curves have been obtained from $FLI^{\pm}_{\phi_2}$: the bold blue curve Λ^2_1 represents $W^c_{C,2} \cap \Sigma_V$, the light blue curves represent the $\Lambda^2_2, \ldots, \Lambda^2_6$. In the bottom panels we zoom in the red boxes. From the zooms, we notice an additional ridge, which is the $\tilde{\Lambda}^1_4$ discussed in the text, connected to the Λ^1_4 through the planar ridge λ^1_4. Both ridges $\Lambda^1_4, \tilde{\Lambda}^1_4$ are represented in orange in the bottom panels.

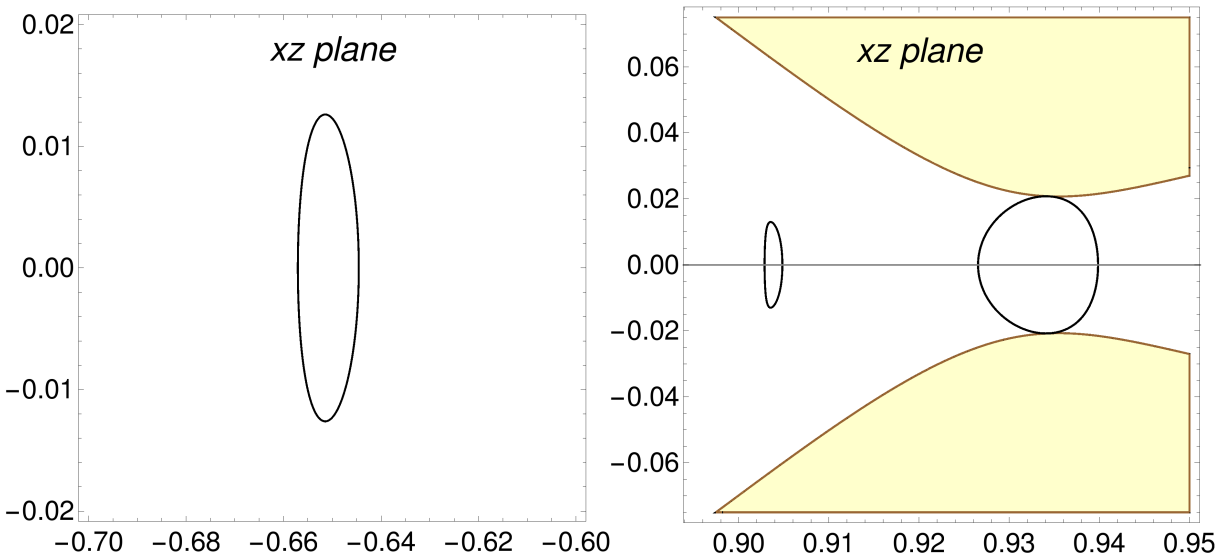

Figure 7: **Intersection of $W^s_{C,1}$ with the vertical section Σ_V in the realm S.** The light black curves represent the ridges M^1_1 (left panel) and M^1_2 (right panel).

close to the ridges of the chaos indicators previously computed.

We first represent the tube of orbits with initial conditions on the ridges Λ^i_j of the modified FLIs. Ideally, these orbits converge to the center manifold $W^c_{C,i}$ for both positive and negative times; but, since the ridges approximates the stable/unstable manifolds up to a numerical error, which in this case is $\varepsilon_1 \sim 10^{-14}$, the orbits approach and remain close to $W^c_{C,i}$ only up to some finite time T. In figures 9 and 10 we represent the tubes generated by Λ^1_2 and Λ^1_4 respectively: in the top panels we represent the projection of a sample of orbits on the xy (top-left) and the xz (top-right) planes; the orbits represented in bold-red are on the planar section of the lobes, while the orbits represented in bold-blue are close to the 'cusps' of Λ^1_4. We notice the sense of rotation around P_2 of the orbits, which is anti-clockwise, until they enter the realm R_1, where they change their rotation sense to follow a clockwise rotation around the center manifold. In the bottom panels we represent the projection of the tubes on the three dimensional space xyz.

Even if the numerical error is very small, by extending the integration time these orbits will transit through the bottleneck of $\mathcal{B}_C$ at L_1 or bounce back, depending on which side of the stable manifold they actually are. As a matter of fact, the meaning of the numerical computation of each curve Λ^i_j is the determination of an annulus $\sigma^i_j \subseteq \Sigma_V$ delimited by an inner curve and an outer curve, whose points are at distance from Λ^i_j larger than the numerical error ε_1. Therefore, with the exception of the points of the annulus σ^i_j, we are able to

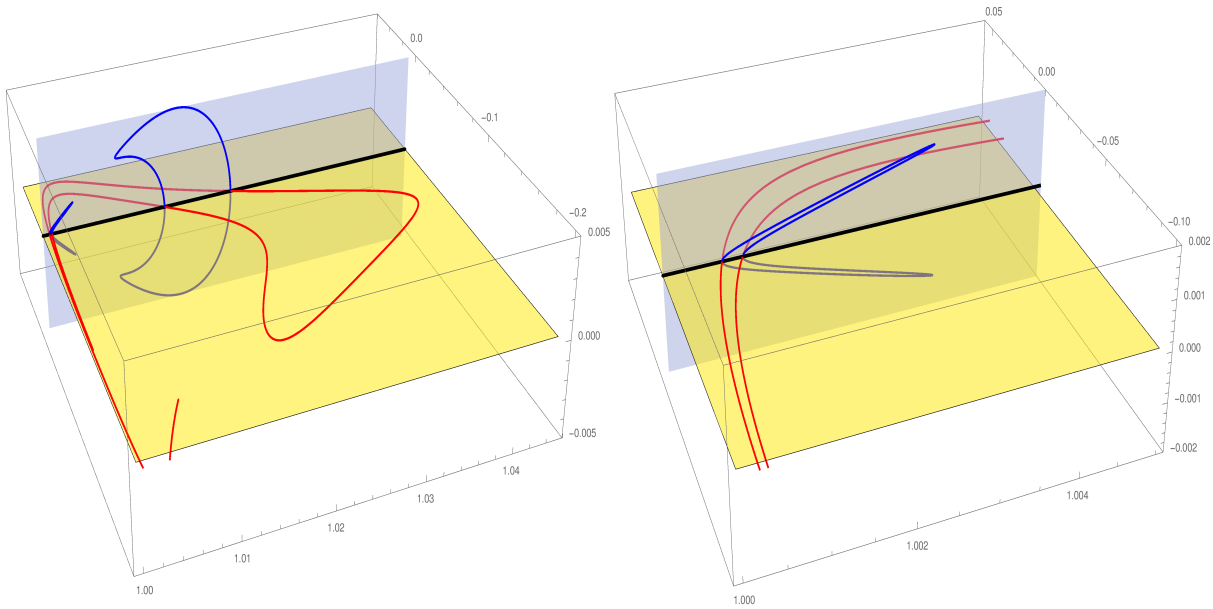

Figure 8: **Intersection of the ridges $\Lambda_4^2, \tilde{\Lambda}_4^2$ with λ_4^2.** The ridges $\Lambda_4^2, \tilde{\Lambda}_4^2$ of Σ_V and the ridge λ_4^2 of Σ_P are all represented in the same three-dimensional section of the phase-space $\Sigma = \{(x, y, z, \dot{x}, \dot{y}, \dot{z}) : y = 0, \dot{z} = 0, \mathcal{C}(x, y, z, \dot{x}, \dot{y}, \dot{z}) = C\}$. The section is parametrized by the variables $x, z, \dot{x}$, so that the horizontal yellow plane represents the planar section Σ_P, the blue vertical plane represents the vertical section Σ_V. The ridges $\Lambda_4^2, \tilde{\Lambda}_4^2$ are clearly connected by λ_4^2.

identify with numerical error ε_1 the interior and the exterior of the tubes of orbits generates by $W^s_{C,i} \cap \Sigma_V$. The dynamics of orbits with initial conditions in the tubes approximated by a Λ^i_j is such that, after $(j-1)/2$ circulations around P_2, the orbits transit to the internal realm S, if $i = 1$, or to the external realm E, if $i = 2$. In figure 11 we report the different time evolutions of the internal and external borders of the two annuli σ^1_2, σ^2_4 (whose borders have distance $\varepsilon = 10^{-10}$ from λ^i_j; we selected ε much larger than the numerical precision, to appreciate the dynamics of all the orbits on the border in short times): for $i = 1, 2$ all the orbits in the inner border, after some circulations of the center manifold, transit to S, E respectively; all the orbits in the external border, after some circulations of the center manifold, bounce back to the realm J.

The transit properties of orbits which are external to the tubes is in part uncertain, since there can be different branches of Λ^i_j (see figure 8) which are disconnected in Σ_V but are connected through Σ_P: an initial condition which is external to a connected component of Λ^i_j, but internal to a different connected component of Λ^i_j, transits to the realm S in $(j-1)/2$ circulations. Therefore, while the dynamics of the inner border of the σ^i_j is certainly determined, the dynamics on the external border of σ^i_j is determined for a certain integration time T only if the error ε_1 is suitably small. Global snapshots of the transit

properties from the realm J to the realms S, E are provided in figure 12. For any initial condition on a refined grid of 10000×2000 initial conditions of Σ_V we computed their orbits until they reach a value for the x coordinate smaller than 0.933 or larger than 1.067. In the former case, we represent the initial condition with a violet pixel, in the latter we represent the initial condition with an orange pixel. If none of the conditions is met in a certain fixed integration time T, we represent the initial condition with a yellow pixel. Though such representations have a poor precision with respect to the FLIs computations (here, the precision in separating the interior from the exterior of a tube is provided by the step-size of the grid, and is 9 orders of magnitude worst than the FLI computations), they provide a snapshot of the global dynamics on the section Σ_V.

7 Conclusions

The global computations of the manifolds asymptotic to the center manifolds originating at the Lagrangian points L_1, L_2 is a problem at the frontier of the dynamical systems science; in fact, in addition to usual numerical difficulties induced by hyperbolic dynamics, the gravitational singularities determine a non trivial geometry of the phase-space and a source of numerical limitations. Geometric regularizations, such as the Kustaanheimo-Stiefel regularizations, provide excellent solutions to the numerical issues, but introduce hidden gauge symmetries with subtle consequences. In this paper, we abandon the traditional way of computing the asymptotic manifolds for a strategy based on the use of chaos indicators. We had to formulate from scratch the variational theory related to the Kustaanheimo-Stiefel regularizations, especially to study the relationship with the orbits in the physical phase space. We found natural to define the chaos indicators in a geometric framework, by exploiting all the properties of the gauge symmetry. The applications of these ideas to the Sun-Jupiter case have provided new insights about the structures of the asymptotic manifolds as well as of the dynamics in the vertical section Σ_V. We plan in the future to consider further extension of this theory, by including perturbations of the spatial three-body problem, such as elliptic problems or perturbations from an additional massive body.

Acknowledgments

We are deeply grateful to Claude Froeschlé, who suggested us in 2008 to define chaos indicators using the KS transformation. We needed eight years to fill the gaps between some promising numerical results produced at the time and the

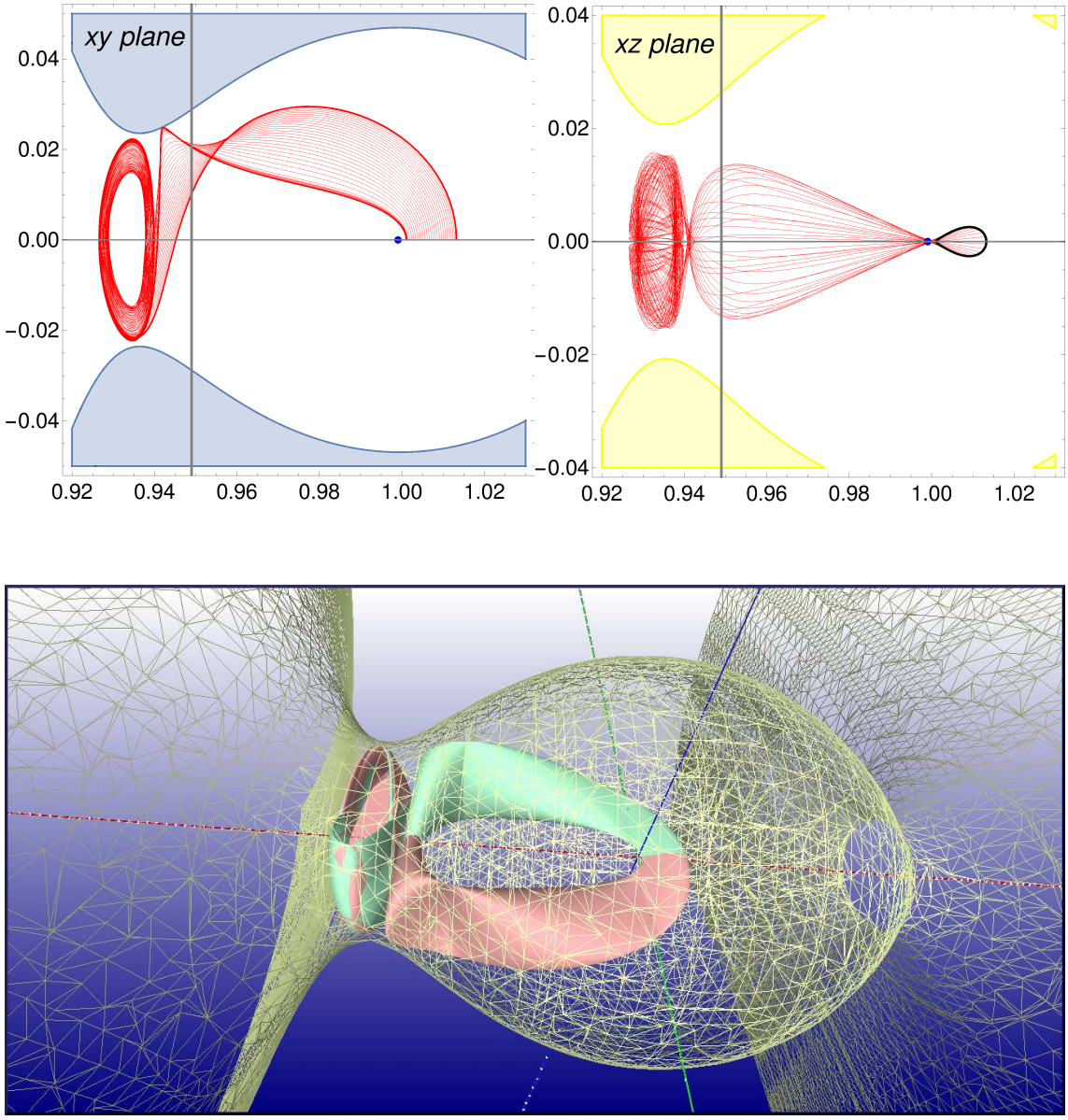

Figure 9: **Geometry of the tube generated by Λ_2^1.** A sample of orbits in Λ_2^1 has been integrated forward in time. The top-left panel represents the projection of these orbits on the xy plane (the the two orbits represented in bold are on the planar section of the lobe); the top-right panel represents the projection of these orbits on the xz plane. The light-blue and the yellow regions represent the forbidden regions in the plane xy and xz respectively. Then, the same initial conditions have been integrated backward in time. In the bottom panel we represent in the three–dimensional space xyz the mesh generated by the orbits obtained with the forward integration (represented in green) and with the backward integration (represented in pink). The transparent mesh represents the border of the real of the forbidden motions. The pink disk inside the center manifold is a surface whose border is the Lyapunov orbit LL_1.

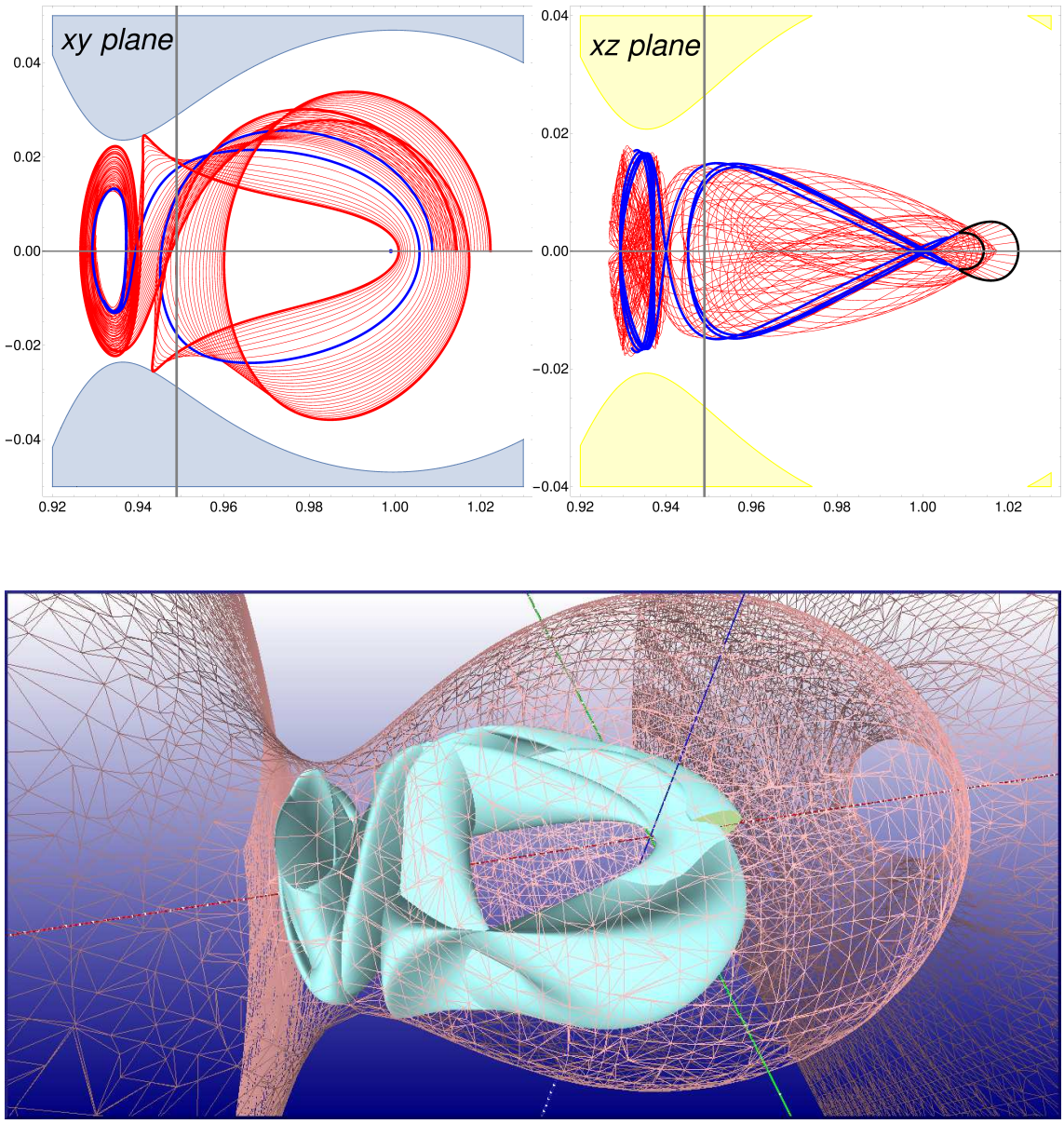

Figure 10: **Geometry of the tube generated by Λ_4^1.** A sample of orbits in Λ_4^1 has been integrated forward in time. The top-left panel represents the projection of these orbits on the xy plane, the top-right panel represents the projection of these orbits on the xz plane (the two orbits represented in red-bold are on the planar section of the lobe; the two orbits represented in blue have initial conditions close to the 'cusps' of λ_4). The light-blue and the yellow regions represent the forbidden regions in the plane xy and xz respectively. In the bottom panel we represent in the three dimensional space xyz the mesh generated by the same orbits (represented in light blue). The transparent mesh represents the border of the forbidden region.

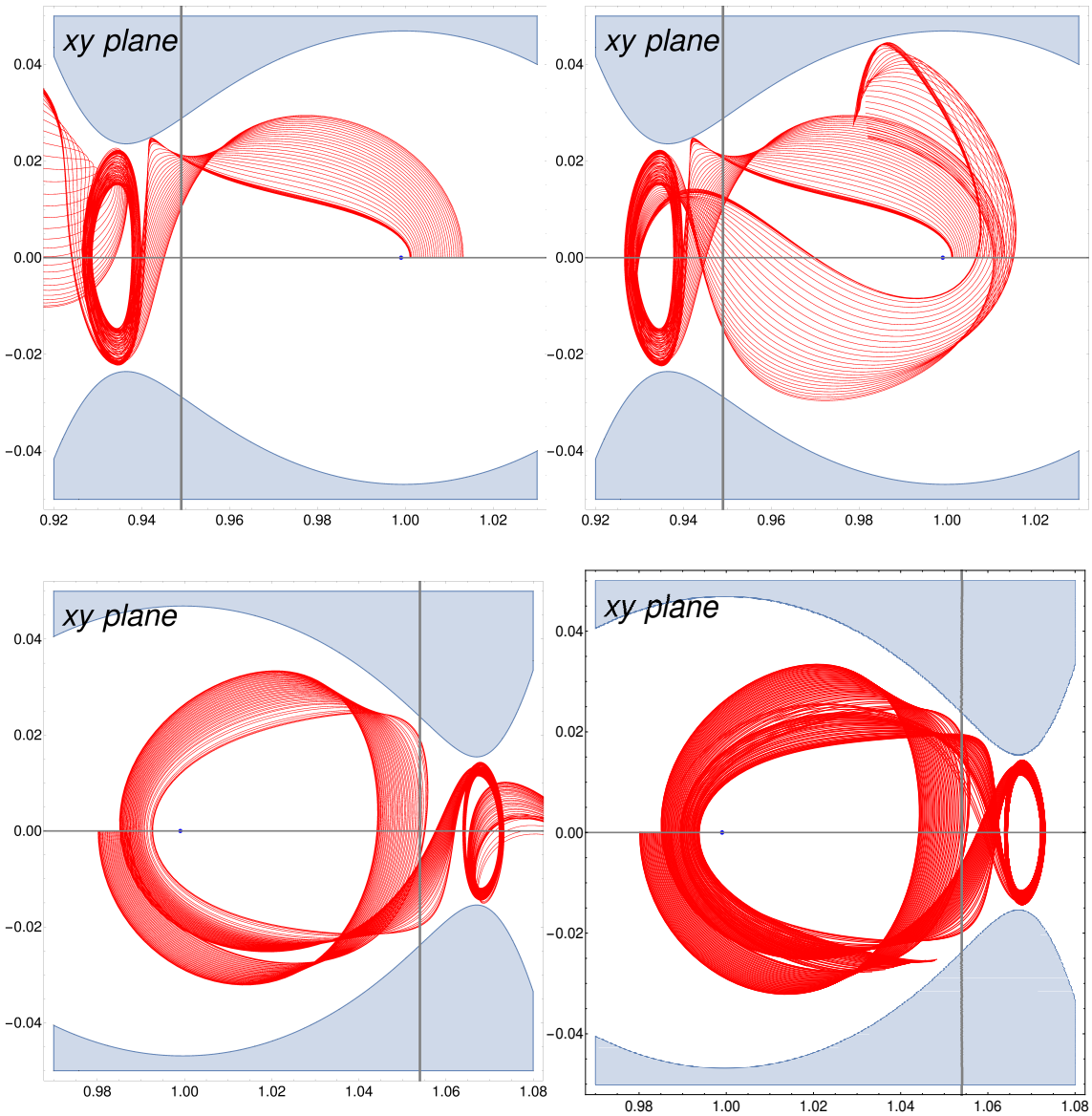

Figure 11: **Evolution of orbits with initial conditions on the annuli σ_2^1, σ_4^2.** We represent the projection on the xy plane of orbits with initial conditions in a sample of the inner border (top-left panel) and outer border (top-right panel) of σ_2^1, and on the inner border (bottom-left panel) and outer border (bottom-right panel) of σ_4^2.

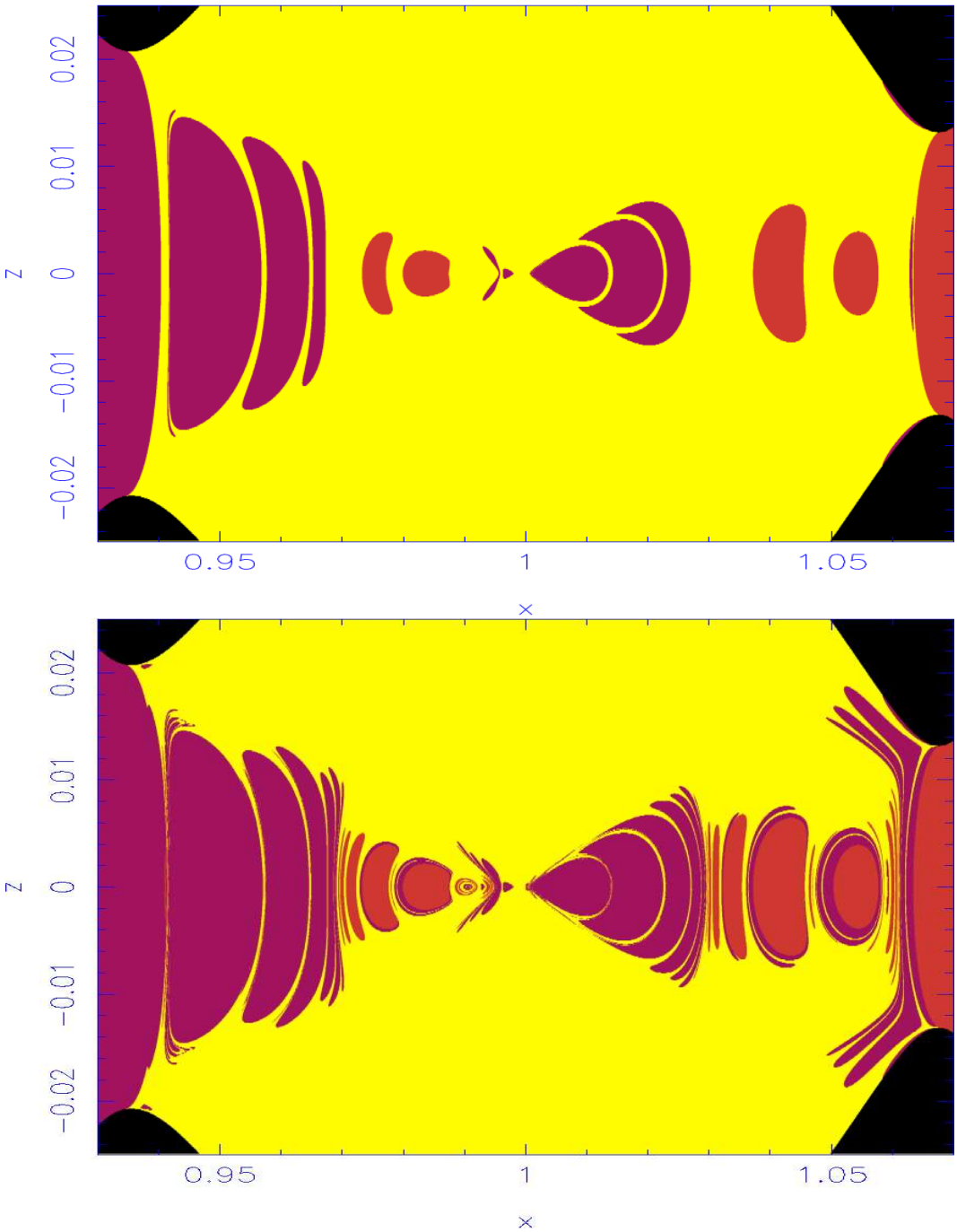

Figure 12: **Transits from the realm J to the realms S, E.** For any initial condition on a refined grid of 10000×2000 initial conditions of Σ_V we computed their orbits until they reach a value for the x coordinate smaller than 0.933 or larger than 1.067. In the former case, we represent the initial condition with a violet pixel, in the latter we represent the initial condition with an orange pixel. If none of the conditions is met in a certain fixed integration time T, we represent the initial condition with a yellow pixel. The top panel has been obtained with the integration time $T = 5$; the bottom panel with the integration time $T = 10$.

results here reported, but without Claude's intuition the present paper would not exist.

M. Guzzo gas been supported by the project CPDA149421/14 of the University of Padova "New Asymptotic Aspects of Hamiltonian Perturbation Theory". Part of the numerical computations have been done on the "Mesocentre SIGAMM" machine, hosted by the Observatoire de la Côte d'Azur. The three-dimensional graphics of figures 3,5,9,10 have been produced using the software Meshlab, by Visual Computing Lab-ISTI-CNR, *http://meshlab.sourceforge.net/*, (a tool developed with the support of the 3D-CoForm project).

References

[1] Aarseth, S. J., Direct Integration Methods of the N-Body Problem, Astrophysics and Space Science, vol. 14, issue 1, pp. 118-132, 1971.

[2] Aarseth, S. J., Gravitational N-Body Simulations, Cambridge University Press, 2003.

[3] Bettis D. G. and Szebehely V., Treatment of Close Approaches in the Numerical Integration of the Gravitational Problem of N-Bodies (Papers appear in the Proceedings of IAU Colloquium No. 10 Gravitational N-Body Problem (ed. by Myron Lecar), R. Reidel Publ. Co. , Dordrecht-Holland.), Ap & SS, 14, 133, 1971.

[4] Conley C., Low Energy Transit Orbits in the Restricted Three-Body Problems. SIAM J. Appl. Math., 16(4), 732746, 1967.

[5] Conley C., Easton R., Isolated invariant sets and isolating blocks, Transactions of the American Mathematical Society 158, 35–61, 1971.

[6] Froeschlé C., Numerical Studies of Dynamical Systems with Three Degress of Freedom, Astron. & Astrophys., vol. 4, 115-128, 1970.

[7] Froeschlé C., Lega E. and Gonczi R., Fast Lyapunov indicators. Application to asteroidal motion, Celest. Mech. and Dynam. Astron., 67, pp. 41–62, 1997.

[8] Gawlik E.S., Marsden J.E., Du Toit P., Campagnola S., Lagrangian coherent structures in the planar elliptic restricted three body problem, Celestial Mech. Dynam. Astronom., 103, 227249, 2009.

[9] Gomez G., Koon W.S., Lo M.W., Marsden J.E., Masdemont J. and Ross S.D., Connecting orbits and invariant manifolds in the spatial restricted three-body problem, Nonlinearity, 17, 15711606, 2004.

[10] Guzzo M., Chaos and diffusion in dynamical systems through stable–unstable manifolds, in "Space Manifolds Dynamics: Novel Spaceways for Science and Exploration", proceedings of the conference: "Novel spaceways for scientific and exploration missions, a dynamical systems approach to affordable and sustainable space applications" held in Fucino Space Centre (Avezzano) 15–17 October 2007. Editors: Perozzi and Ferraz Mello. Springer. 2010.

[11] Guzzo M., Lega E. and Froeschlé C., A numerical study of the topology of normally hyperbolic invariant manifolds supporting Arnold diffusion in quasi-integrable systems. Physica D,182 , 1797-1807, 2009.

[12] Guzzo M., Lega E., On the identification of multiple close-encounters in the planar circular restricted three body problem." Monthly Notices of the Royal Astronomical Society, 428, 2688-2694, 2013.

[13] Guzzo M., Lega E., Evolution of the tangent vectors and localization of the stable and unstable manifolds of hyperbolic orbits by Fast Laypunov Indicators, SIAM J. APPL. MATH., Vol. 74, No. 4, pp. 10581086, 2014.

[14] Gómez G., Jorba À., Masdemont J., Simó C., Dynamics and Mission Design Near Libration Point Orbits, Vol. 3: Advanced Methods for Collinear Points, World Scientific, Singapore, 2000.

[15] Jorba A., Masdemont J., Dynamics in the center manifold of the restricted three-body problem, Physica D 132, 189213, 1999.

[16] Koon W.S., Lo M.W., Marsden J.E. and Ross S.D., Dynamical Systems, the three body problem and space mission design. Marsden Books. ISBN 978-0-615-24095-4, 2008.

[17] Kustaanheimo P., Spinor regularisation of the Kepler motion, An- nales Universitatis Turkuensis A 73, 1-7. Also Publications of the As- tronomical Observatory Helsinki 102, 1964.

[18] Kustaanheimo P. and Stiefel E.L., Perturbation theory of Kepler motion based on spinor regularization, Journal f ur die Reine und Angewandte Mathematik 218, 204-219, 1965.

[19] Haller, G., Distinguished material surfaces and coherent structures in three-dimensional fluid flows, Physica D 149, 248277, 2000.

[20] Haller, G., Lagrangian coherent structures from approximate velocity data. Physics of Fluids, 14 (6), 18511861, 2002.

[21] Hopf H., Math. Ann., 104, 637, 1931.

[22] Lega E., Guzzo M. and Froeschlé C., A numerical study of the hyperbolic manifolds in a priori unstable systems. A comparison with Melnikov approximations, Cel. Mech. and Dyn. Astron., 107, pp. 115-127, 2010.

[23] Lega E., Guzzo M. and Froeschlé C., Detection of close encounters and resonances in three-body problems through Levi-Civita regularization, Monthly Notices of the Royal Astronomical Society, vol. 418, 107-113, 2011.

[24] Lega E. and Guzzo M., Three-dimensional representations of the tube manifolds of the planar restricted three-body problem, Physica D, vol. 325, 41-52, 2016.

[25] Lekien, F., Shadden, S.C., and Marsden, J.E., Lagrangian coherent structures in n-dimensional systems. Journal of Mathematical Physics, 48, 065404, 2007.

[26] Levi-Civita T., Sur la régularisation du probléme des trois corps, Acta Math., vol. 42, 99-144, 1920.

[27] Moeckel R., Isolating Blocks Near the Collinear Relative Equilibria of the Three-Body Problem, Transactions of the American Mathematical Society 356, 4395-4425, 2004.

[28] Mikkola S., Few-Body Problem: Theory and Computer Simulations, Annales Universitatis Turkuensis, Series 1A, Vol. 358, C. Flynn, ed., 2006.

[29] Peters C. F., Numerical Regularizations, Bull. Astron., 3, 167, 1968.

[30] Roy A. and Ovenden M.W., On the occurrence of commensurable mean motions in the Solar System II, The mirror theorem, Mon. Not. Roy. Astr. Soc. 115, pag. 296, 1955.

[31] Shadden S.C., Lekien F. and Marsden J.E., Definition and properties of Lagrangian coherent structures from finite-time Lyapunov exponents in two-dimensional aperiodic flows, Physica D 212, 271304, 2005.

[32] Sijbrand J., Properties of Center Manifolds, Transactions of the American Mathematical Society, vol. 289, n. 2, pp. 431-469, 1985.

[33] Simó C., Dynamical systems methods for space missions on a vicinity of collinear libration points, in Simó, C., editor, Hamiltonian Systems with Three or More Degrees of Freedom (S'Agaró, 1995), volume 533 of NATO Adv. Sci. Inst. Ser. C Math. Phys. Sci., pp. 223-241, Dordrecht. Kluwer Acad. Publ., 1999.

[34] Szebehely V., Theory of orbits. Academic Press, New York, 1967.

[35] Sundman K. F., Acta Math., 36, 105, 1912.

[36] Waldvogel J., Fundamentals of Regularization in Celestial Mechanics and Linear Perturbation Theories, in Extra-Solar Planets : The Detection, Formation, Evolution and Dynamics of Planetary Systems, B. Steves, M. Hendry, A.C. Cameron editors, CRC Press, Taylor and Francis group, 2001.

[37] Tang X.Z., Boozer A.H., Finite time Lyapunov exponent and advectiondiffusion equation, Physica D 95 (1996) 283305.

[38] Villac B.F., Using FLI maps for preliminary spacecraft trajectory design in multi-body environments, Cel. Mech. and Dyn. Astron., 102, pp. 29–48, 2008.